

Calving event size measurements and statistics of Equip Sermia, Greenland, from terrestrial radar interferometry

Andrea Walter, Martin P. Lüthi, Andreas Vieli

5

Submitted for review to The Cryosphere in May 2019

Reply to reviewer's comments

10

General reply

15 We thank both reviewers, Surui Xie and Pierre-Marie Lefeuvre, for reading through the manuscript and their critical comments and helpful ideas, and suggestions. We appreciate the invested time for their feedback. The reviewer's major concerns mainly refer to the issue of uncertainty in TRI derived elevation models, the ice flux budget estimation and the statistical analysis. We are thankful for these comments and we addressed those comments in our revisions and think that they considerably improved our manuscript.

20 The main changes we undertook are:

- using an additional threshold to reduce the distortion in the shallow sector.
- a detailed error analysis of the stable terrain between the TRI derived DEMs.
- a comparison of the ArcticDEM with the TRI derived DEMs.
- a more detailed analysis of the ice flux as comparison to the calculated calving volumes.
- 25 - and all minor corrections and editing issues have been addressed.

Reply to major concerns Referee 1

30

Uncertainty in TRI derived elevation models needs better assessment. The authors randomly choose 30 DEMs and computed the variability (its definition needs to be provided in the manuscript) as a measure of the precision.

35 Although the mean variability is 1 m, but the maximum variability is 5 m. Therefore, the DEMs are likely to have an uncertainty of ~1 m to several meters. Although a threshold of 5m elevation decrease between adjacent DEMs is used to determine calving events, but note that even among only 30 DEMs there is a variability of 5 m between two DEMs. The calving statistics of this manuscript come from hundreds of DEMs, several large random errors (2σ or above) or outliers can significantly change the results. I suggest the authors to provide more details on error analysis.

40

We agree that the uncertainty analysis was presented too vaguely. We added section 4.1 on the resulting DEMs and error analysis. Additionally, we added Figures S2, S3 and S4 showing the variabilities on stable terrain over space and time. The test area on stable terrain is indicated now in Figure 3 as a yellow box. It is important to note, that this more detailed error analysis does however not substantially change our results and main findings stated in the paper.

Based on the calving data derived from TRI elevations, the authors concluded that surface calving is more frequent in the shallow water sectors, and the sizes are generally larger. This seems apparent if just looking at Figure 5c. However, due to lack of rigorous uncertainty analysis, I think this conclusion is hasty and may be flawed. In general, noise in TRI measurements increases with distance, and can increase rapidly at a distance of 4-6 km. Glacier front on the northwestern section (shallow water sectors in this manuscript) is further from the radar than the southeastern section (deep water sector), thus radar data on the northwestern section of the glacier should be noisier if all other conditions are similar.

Besides, the northwestern section of the glacier front is crevassed heavier than the southeastern section (Figure 1), and elevation changes rapidly (inclined at a slope of 50 degrees according to the authors), both are more likely to induce phase unwrapping errors than a flat and less crevassed surface. These (i.e., increased noise with distance, phase unwrapping problems) could be some of the reasons why the identified calving volumes are more variable and the cumulative calving volumes are larger along the SL/SM/SR/M sectors. In Figure 5c, timing and sizes of calving events at different distances look random, but considering the characteristics of radar noise, it is important to examine if the observed pattern is due to noise or unwrapping errors. Here I suggest one possible method to test how much noise affected the distribution pattern in calving events: using the same analysis approach as presented in the manuscript, but apart from calculating calving volume based on pixels whose elevation decreased by >5 m, the authors can also calculate "increased volumes" by pixels whose elevations increased by >5 m. If a similar distribution pattern as in Figure 5c is seen, then the derived "calving volumes" are likely disturbed. The authors can probably add a plot of such "increased volumes" to the negative side of y-axis in Figure 5d (can use light blue color if the authors don't want it to be distracting). A comparison figure of "detected increasing volume" similar as Figure 5c can also add important information to the manuscript, and it can go to the supplement if the authors would like to save space in the main manuscript.

We realized that in our paper the correction process to minimize errors with distance is not described. However, we used a correction factor to correct for systematic error sources. Those error sources can be caused by errors in the reference heights and instrumental geometry, baseline errors and errors caused by a not perfectly vertical mounting of the three antennas (Strozzi et al., 2012). We did that by comparing the calculated DEMs with the Arctic DEM and choosing control points on stable terrain at different distances from the radar. With the used correction factor we can minimize uncertainty in the height estimates. We added this information to the DEM generation methods (section 3.1). Considering the geometry of the calving front we agree that the shallow sector is more likely to induce errors than the deep part with the less steep front geometry. We thank referee 2 for his suggestion of doing the whole analysis for positive height changes. By investigating the positive changes we realized that the distortions are indeed higher for the shallow sector. Thus we redid the whole analysis and added an additional condition in the watershed segmentation algorithm. As the noise has mostly an irregular shape, while the calving events are more homogenous the new extracted events have to fulfil

the condition (number of pixels of event * 1.6) \geq (number of pixels in bounding box) if they are smaller than 40 pixels. This results in a smaller number of extracted calving events but it is less sensitive to noise. We included a positive volume change graph in the appendix (Fig. S6).

5 After our re-analysis as suggested by the referee 1 the main differences between the shallow and deep part in terms of calving remain, even if less calving events were extracted.

10 According to the authors, there was very little surface calving observed by TRI at sector D (the deep water sector), and mass loss due to subaqueous calving is dominant (50% or more, depends on the rate of oceanic melt) here. Limited evidence of subaqueous calving was shown in the manuscript. Even if substantial subaqueous calving events occurred and contributed significantly to the mass loss at the deep water sector, the manuscript failed to explain where the mass goes. I also think it is not adequate to simply assume that subaqueous calving is independent of TRI observed surface calving. If subaqueous calving would not cause surface elevation change by following the authors' logic, then what was there to fill the space left by the "subaqueous calving"? Besides, if TRI observed little calving at sector D, then glacier front at this section should advance, especially at the high velocity area. 15 Speed in the middle of this sector is 16 m/day, in ~7.65 days, ice front here can advance over 100 meters, much larger than the resolution of either Landsat/Sentinel satellites or TRI images so should be detectable. However, Supplementary Figure S1 rejected this.

20 We agree that the explanation of the processes happening at the deep sector was not complete. We cannot see subaqueous calving events with the TRI data but we added images of a subaqueous calving event from the time-lapse camera installed in 2018. Unfortunately, no time-lapse camera was installed in 2016. As the flow field and surface slope further upstream is homogenous (smooth across-flow profile velocity profile) and thereby does not indicate substantial differences in ice thickness we assume that the ice thickness downstream (towards the front) is similar for the shallow and the deep sector also at the calving front. We argue that if this assumption would not hold, we would see it in the surface structure of the glacier by specific crevasses or flow velocity variations. Thus, if the ice thickness is similar, at the deep sector about 45 % - 65 % of the ice area are below the waterline. The remaining missing volume might be calved off above the water line through small calving events, which were filtered out during the analysis. Those small events can be caused by undercutting of the calving front due to ocean melt and calving below the waterline. We calculated now the flux with the available front height and velocity and also with an assumed ice thickness of 150m. This estimated flux is included in Figure 7. 25 30

35 The manuscript did not explain the method they used to choose the study area for calving detection well. Although on page 6 the authors mentioned that they applied a mask with ~150 m wide across the glacier front, however, the glacier front was constantly moving, so a Lagrangian frame should be used. Whatever the reference frame was, according to the methods presented by the authors, areas with calving event detected (Figure 4) over the center of sector D should have the largest along-flow direction width. This is because glacier front at this location should advance (also see comment above), thus the test area should move. Whereas Figure 4 shows a different pattern. 40

45 We added a figure showing the used front position mask and an example from the watershed algorithm. The front position advanced and retreated only marginally but was always well within the mask. Thus we decided to use a simple constant mask. The fact that the centre of sector D does not

have the largest along-flow direction width we explain with many small events, which might be triggered by undercutting of the calving front due to underwater calving and ocean melt.

5 **Detailed comments:**

Page 2, line 4: “was” → “were”, data should be plural.

We adjusted this accordingly in the revised manuscript. Additionally, we changed data to plural in the whole manuscript.

Page 2, line 6: “style” → “styles”.

10 We corrected this in the revised manuscript.

Page 2, line 8: “missing” → “deficiency” ?

We changed this in the revised manuscript.

Page 2, lines 8-10: later in the manuscript, one conclusion was that that subaqueous calving and oceanic melt combined contribute ~75% to the frontal mass loss. However, here it seems that
15 subaqueous calving itself contribute up to 75% of the frontal mass loss. Please clarify.

We rephrased this sentence and hope that it is clearer now.

Page 2, line 18: It would be great if the authors can be more specific about “water masses in Greenland”. Did the authors mean “water masses around Greenland”, or “increase in surface water due to melt”?

20 Straneo et al. (2013) suggested that a warming of the subpolar North Atlantic together with an increased runoff lead to enhance submarine glacier melting. So here we meant water masses around Greenland. We changed it to “water masses around Greenland”.

Page 2, line 21: What are the major remaining limitations? A few examples briefly listed here would be helpful.

25 Examples would be that the link between atmospheric forcing and calving activity is not straightforward and that with the currently available resolution in models and observations small scale processes like subglacial hydrology are not resolvable or that short term and long term observations are often not available. We included some examples in the revised manuscript.

Page 2, line 24: I am not sure if calving controls tidewater glaciers’s react to environmental condition
30 changes, or verse visa? Please clarify.

We agree that the sentence was confusing. We changed it in the revised manuscript to: “Calving is a crucial process for the dynamic behaviour of tidewater glaciers, but the detailed mechanisms and

relation to environmental forcing are not well understood (Joughin et al. 2004; Thomas, 2004; Nick et al., 2009).”

Page 3, line 8: “was” → “were”.

We corrected this in the revised manuscript.

5 Page 4, line 7: Figs. 1 and 2.

We changed this in the revised manuscript.

Page 5, line 13: “whole” → “entire”.

We corrected this in the revised manuscript.

Page 5, line 18: “climate” → “weather”.

10 We corrected this in the revised manuscript.

Page 6, lines 16-18: Are these differences RMS difference, Mean difference, or other types? These can be quite different because the difference between TRI-DEM and Arctic DEM can be systematically and/or randomly. Please clarify.

15 The differences calculated here are mean differences but we added a more complete comparison of the TRI-DEM and the Arctic DEM in the revised manuscript in section 4.1 and Figure S7.

Page 6, line 17: Does “variability” mean “repeatability”, or changes of topography? Please clarify.

We extended this section to a more detailed error analysis in section 4.1, where we investigate the variabilities on stable terrain. With variability we mean the difference between two DEMs for points on stable terrain.

20 Page 6, lines 17-18: How stable/random is stable/random? Maybe outline the test area in one of Figures 1, 2 or 3? And what does the “values” in line 18 mean? Values of a selected area (if so, please outline it in Figure 1/2/3) or selected DEMs (if so, maybe mark the times in Figure 5c)?

We extended this analysis in section 4.1. The test area on stable terrain is marked in Figure 3.

25 Page 6, lines 23-24: Does the “10 pixels” mean “10-adjacent pixels”? I feel the two numbers “10 pixels” and “3 pixels” are confusing: Does noise needs to fulfill both “area<10 pixels” AND “width<3 pixels”? If so, how about a block with 3×3 (9 pixels, each pixel shown by an “O” below) shape like

“ OOO

OOO

OOO”, or a 2×8 shape like

30 “ OOOOOOOO

OOOOOOOO ”, or a shape like

“ OO

OOOOO

OOOO ”

- 5 Are these considered calving events if all “O” pixels have elevation decreases more than 5 m? Because many of the identified calving events are quite small, and shapes of these blocks may not be regular, I think it is important to clarify these settings here.

We agree with referee 1 that the settings for the thresholds need to be clarified more to avoid confusion. Calving events need to fulfil both conditions, a size of 10 adjacent pixels and a width of 3 pixels. For the width it is enough if the bounding box has 3 pixels. All the pixels need to have an elevation decrease of more than 5 m, except if some pixels with a lower decrease are surrounded by pixels with a decrease of more than 5 m. Then those pixels are included in the calving event. So a 3x3 and a 8x2 shape are not considered as calving event but the third shape you mention is extracted as calving event.

- 15 In the revised manuscript we changed the description accordingly to: “Additionally, calving events smaller than 10 adjacent pixels and with a bounding box width smaller than 3 pixels were excluded as noise. Thus only calving events with both, ≥ 10 adjacent pixels and a bounding box width larger than 3 pixels, were extracted.”

- 20 Page 6: Apart from using elevation changes to detect calving, it is also possible to identify calving from radar amplitude images. Including an example showing both changes in radar amplitude and elevation would be strong evidence that the method is reliable.

Instead of including an example of identifying calving from radar amplitude images we added in the supplement an example of a calving event which is visible on the multi-look radar images (Fig. S5).

- 25 Page 7, lines 5-6: Did the authors mean that p should always be larger or equal to 0.1, or did they mean that one can only trust the sign of R when $p \geq 0.1$? If it is the latter, maybe rewrite the sentence to “which tells if one can trust the sign of R (when $p \geq 0.1$)”?

We changed the sentence to “which tells if one can trust the sign of R (when $p \geq 0.1$).”

Page 7, line 15: Please also specify the low-pass frequency. Just as how the high-pass frequency was given.

- 30 The pass frequency for the low-pass filter was 0.001 Hz. We added that to the revised manuscript.

Page 7, line 19: To avoid confusion for readers who are not familiar with radar, I suggest to add “line-of-sight” in front of “shadow”.

We added “line-of-sight” in front of “shadow”.

Page 7, lines 26-28: I found that the number of total identified calving events is smaller than the sum of identified calving events in the shallow sector and the deep sector ($1681 < 1403+289$). Did I miss anything? Please also check numbers in Table 1, many of them are not consistent.

- 5 The number of total identified calving events is smaller than the sum of identified calving events in the shallow and the deep sectors, because 12 events happened to be located on the boarder of the two sectors. Those events were counted only once for the total number but for both the number of the shallow and the number of the deep sector (double counting).

- 10 We added an explanation to this in the revised manuscript on page 8, line 6-7: “Note that 12 events were detected on the border of the two sectors and were thus counted for both sectors but only once for the total number of events.”

- 15 Page 8, line 2: Please ensure the minimum size of identified calving block fulfill the threshold defined for calving events (based on lines 21-24, page 6, I calculated a minimum volume $5 \times 10 \times 3.75 \times 3.75 = 703$ m³. Or did I misunderstand the “resolution”? — I picked it from line 13, page 6. Using the radar pixel specified in line 6 page 8 the minimum volume of identified block is even larger, i.e., 1500 m³). If this paper aims to do statistics of calving event sizes, please ensure that the statistics are correct.

- 20 We thank referee 1 for spotting this. We realized that some of the events were considered as calving events even if they are collapsing seracs upstream on the glacier surface. They were included as they were located exactly on the border of our glacier front mask. Those events are excluded in the revised manuscript. The removal of those small events influences the calving size distribution but all the other results and the main conclusions are not affected.

The algorithm takes also events into account where pixels of less than 5 m decrease are surrounded by pixels of more than 5 m decrease. Thus the events can be smaller than the calculated minimum size of a calving event.

- 25 Page 8, lines 6-9: I think to calculate cumulative calving height a Lagrangian frame needs to be used, because ice at the front can move at 16 m/day (line 21 on page 7), which means a ~100 m displacement during the observation period. If the authors were referring to cumulative calving height from calved ice height at each pixel in each calving events, then line 6 needs to be rewritten, at least taken away “differences” because calved height was estimated from the difference between two DEMs.

- 30 We added a figure in chapter 4.1 showing an example of the watershed algorithm and also the used front mask. In figure S1 it becomes visible that the front is changing its position only marginally. Thus using a constant mask seems to be appropriate.

We changed the sentence to “Calving heights in each radar pixel..” in the revised manuscript.

Page 8, line 8: If cumulative calving height exceeds 300 m but not up to 300 m, please

consider using “extend=‘max’” for the color bar of Figure 4.

We changed the Figure accordingly and used extend=max in the color bar.

5 Page 8: I think TRI-derived DEMs in this paper are very important data, however, there was no figure showing the DEM, neither in the main paper nor in the supplement. Please consider to include a TRI-derived elevation map in the manuscript. Maybe add a panel or two in Figure 3?

We included Figure 3 of a TRI-derived DEM in section 4.1.

10 Page 9, Figure 4: Comparing this figure with the text makes me confused. If ice velocities on the two sides of sector M are the fastest (see Figure 3) but cumulative calving heights are not the largest (see colormap in Figure 4), shouldn't these two areas have the widest (along flow direction) spatial distribution of calving events? Please check data processing, and make sure the descriptions in lines 25-27 on page 6 are correct.

The calving front only changed marginally during the observation period. We explain the missing volume for sector M with small calving events, which we cannot detect with our method. We added this explanation to the discussion in section 5.1.

15 Page 9, Table 1: Please check calculations and make sure that numbers are consistent in the table and the main text. In the table, please at least ensure numbers in “Total event volume” equal to “Total event number” × “Mean event sizes”, unless a different math was used.

The numbers in table 1 are rounded as a more detailed number makes no sense due to the uncertainty. So the “Total event volume” equals to “Total event number” x “Mean event sizes”.

20 Page 10, Figure 5: I like this figure! But I also have a few questions and suggestions. First, color changes from dark blue to light blue in Figure 5c is distracting, I suggest to mask out periods without calving using white or grey. In this way, calving characteristics will be more accessible. Consequently, the minimum value of the color bar can be changed to the smallest volume detected based on the settings (lines 20-25 on page 6). Second, I am confused by the right axis of Figure 5d.
25 Can the authors elaborate on this? Third, I could hardly read the superscripts in y-axis label of Figure 5d due to low resolution. Based on the manuscript I guess it was “106 m³” in the bracket, is this correct? Please increase the figure resolution. Also, maybe add “Cumulative” to the y-axis label of Figure 5d to distinguish from the color bar label in Figure 5c. Fourth, I found that the further analysis separates these sectors, so it is necessary to show the exact along-distance ranges of different
30 sectors. Maybe use vertical bars to mark the boundaries of different sectors? These bars can go between the annotations in Figure 5c, such as “| SL | SM | SR | M | D |”. Last, would it be possible to add a narrow column on the right of Figure 5c and show total calving volume along the entire calving front in color? Such a plot may provide useful information on calving volume changes with time.

35 We thank referee 1 for the suggestions. We changed the colours in the Figure 7c. We added cumulative to the y-axis of Figure 7d and we increased the resolution. Also the vertical bars to mark the boundaries of different sectors was included. We did not add a narrow column on the right of Figure 7c as we think this would be too much information for one figure. Also this information is already included in Figure 12.

Page 11, line 4: “already observed” → “shown”

We changed this in the revised manuscript.

Page 11, line 10: It is probably not correct to say “only ... was observed” because small calving volumes are also visible at sector M in Figure 5c. Maybe rewrite to something like “less calving events but several of them are significantly larger than those observed at the other shallow water sectors”.

We rephrased the sentence to: “In the central, very shallow sector M less calving events were observed but several of them are significantly larger than those observed at the other sectors.”

Page 11, lines 11-12: I think there is an ambiguity in “the most individual events”. Maybe rewrite it to “the largest number of calving events”.

10 We rewrote the sentence to “Sector SL with the highest cumulative calving height also has a large number of events,....”

Page 11, line 14: I agree that no clear temporal pattern can be seen throughout the different sectors, it looks pretty much like random noise. Please see my comments above.

With the additional condition we excluded more noise but still have no clear temporal pattern.

15 Page 11, line 15-16: The “observable cluster of calving” is hard to tell from Figure 5c. Yes there are some big events, but since this manuscript does statics, in the sense of statics, do these relatively big events really clustered? Need more elaboration.

We think the observation period is too short to do more statistics. But we will rewrite that this observable cluster is only investigated by looking at it.

20 Page 11, lines 19-21: More detail of deriving the 25% needs to be provided. Is it an appropriate assumption of a constant front position? Here ice can move up to 16 m/day (Figure 3). And the assumption of a constant mass flux over the front also needs to be justified.

We added in Figure 7c two ice flux estimates along the front and adjusted this sentence accordingly. The front position only changed marginally over the whole observation period.

25 Page 11, line 30: A summary of the meaning of the log-likelihood ratio R would be helpful for understanding the statistics. It seems to be an important parameter describing the likelihood of two different models. Also, were there any reasons to choose the three models here? Since one of the major conclusions came from statistics, more details should be provided.

30 We added an explanation on how to understand R in this section. We used the same models as others before as we wanted it to be comparable to other studies. Also this three models are widely used in natural science.

Page 12, Figure 6: In the abstract I found “The size distribution of the deep sector follows a power law, while the shallow sector is likely represented by a log-normal model.” From this figure, could we say

that both can be represented by a log-normal model? The R and p values are identical for the power law and log-normal models in Figure 6d. Or did I miss anything?

With the re-calculated dataset the shallow front follows a log-normal model ($p \geq 0.1$), while for the deep front log-normal and power law model fit well, but none of them significantly better.

- 5 Page 12, line 9: Can the authors provide the unfiltered water level during the entire observation period? So that readers will know the overall characteristics of local water level variations. It can either be in Figure 9, or go to the supplement, maybe add one panel to Figure S2.

The unfiltered pressure sensor dataset is added to the appendix in Figure S9.

- 10 Page 13, line 14: “several clusters of events”? I thought the authors only observed one cluster of calving events (lines 14-16 on page 11). Please clarify.

We thank referee 1 for spotting this. We changed the sentence to “The observed calving events show no temporal or spatial pattern, except for a series of bigger events on 26 August.”

- 15 Page 13, line 15: How did the authors reach to a conclusion that “no clear temporal pattern of tidal or diurnal recurrence could be detected”? Can the authors elaborate? If no evidence, I suggest to omit this sentence. Or at least admit that this is based on the impression of looking by eyes.

We changed the sentence to “The observed calving events show no obvious temporal or spatial pattern, except for a series of bigger events on 26 August”

- 20 Page 13, line 18: I think some of these values can be calculated from the data. If the authors use values derived from real data, the further analysis would sound more reasonable. Also, maybe use “a front thickness” instead of “a front height” to avoid confusion?

We calculated the ice flux in the revised manuscript by using the available elevation and velocity. The calculated flux is added to Figure 7d.

Page 13, lines 18-23 and after: Please try to keep number of digits consistent.

We changed this accordingly.

- 25 Page 13, lines 20-21: Not sure if it is correct to say “This value should match up to ...”? Although the front position looks stable by eyes, but is this sufficient to support an assumption that total ice flux should match observed total calving volume? More rigorous analysis is needed.

We rewrote the whole section as we calculated now the ice flux from the available data.

Page 14, line 1: Remove “with”, add “,” before about.

- 30 We rewrote the sentence in the revised manuscript.

Page 14, line 3: Please check if “160 m³” is correct. And stacking does not likely contribute to the difference unless there are some errors in the data analysis.

As we changed our data analysis this values changed in the new manuscript.

Page 14, line 9: I bet the “ $0.47 \cdot 10^6 \text{ m}^3$ ” correspond to the deep sector? Why assuming an ice thickness of 100 m below the water line? Too many assumptions could result in significant bias. Since the authors have data of surface elevations (shown in Figure 5b), and have assumed a front thickness of 150 m (line 18 on page 13, although I suggested to use real data instead of assumption), ice thickness below water line can be estimated.

We changed that section as we calculate now the ice flux with the available data over the front. Thus by assuming a total ice thickness of 150 m we can calculate also the corresponding ice flux below the waterline. All this information is added to Figure 7d.

Page 14, lines 16-18: If subaqueous calving cannot be detected with the TRI, how could it be detected by visual observations and time-lapse imagery? More details are needed. Maybe show some examples of images taken by the time-lapse camera.

We added an example of a subaqueous calving event recorded with the time-lapse camera in 2018.

Page 14, lines 19-12: I don't think the authors have shown enough evidence to reach this conclusion. If subaqueous calving account for ~50% of the mass removal from the deep sector, the average thickness removed at the glacier front could be calculate by doing simple math. I believe that will lead to significantly mass thickness removal and the deep sector may become afloat by the end. Plus, can the authors see icebergs coming out from subaqueous calving? If it accounts for ~50% of mass loss, then visual observations or time-lapse camera images (line 17) may be able to see icebergs coming out from subsurface. Please provide evidence to support the conclusion.

With the new ice flux calculation this value changed now and it is now 45 - 60 % mass loss is due to oceanic melt and subaqueous calving. We added an example from the time-lapse camera.

Page 14, lines 25-26: If ice cliff at the shallow sector can have larger but stable height, then why do calving events occur so frequently? Although ice here is thicker but calving should be less frequent or no calving at all because ice cliff can be stable (lines 25-26). May the authors were referring to the potential of calving so “a thick cliff CAN release larger ice volumes”, but please note that here calving is quite frequent (also related to how “stable” was defined in this manuscript), while previous figures (e.g., Figure 5c) show that the shallow sectors calved more frequently at the surface. Even add subaquatic calving to the deep water sector, calving at the shallow sectors will still be more frequent than the deep water sector because the authors assumed the overall mass loss are similar in different sectors, plus the deep water sector has lost more mass due to melt.

We changed that sector to explain it better. The vertical front of the deep section might results in smaller events, which are not detectable with the TRI.

Page 15, lines 4-7: Would enhanced submarine melt cause surface elevation decrease because ice becomes thinner? If it won't lead to surface elevation decrease, then what was there to support the upper part of the glacier? Would the empty chambers cause instability and calving? On the other hand, if it will lead to surface elevation decrease, then the TRI might be able to see the decrease. Please clarify.

With the TRI there is no visible decrease in surface elevation due to subaquatic calving. But the subaquatic calving can lead to instabilities and thus to more calving of smaller volumes, which are not detectable with the TRI.

Page 15, line 12: Please show the “Observed subaqueous calving events”. Because the authors wrote that there were time-lapse cameras (line 17 on page 14). If no captured subaqueous calving events by instruments, then please provide more detail of the available observations by authors in the field.

We added an example of a subaqueous calving event recorded with the time-lapse camera in 2018.

5 Page 15, line 19: “acting” —> “dominant”?

We agree with referee 1 that “dominant mechanisms” is more appropriate and changed it accordingly.

Page 15, lines 19-24: The paragraph relies on the assumption that submarine calving in the deep sector is a major contributor to total calving volume. Please evaluate the assumption based on comments above.

10 We added an example of such a subaqueous calving event. The size distribution of the deep sector can be represented by a log-normal and a power law model but no model is significantly better. Thus we reformulated this paragraph and phrased it less certain.

Page 15, line 30: Please explain what is “big up-floating icebergs”. If the icebergs are big, they might appear on the TRI amplitude images. An example image would be helpful.

15 We could not find a nice example on the TRI images as the icebergs often fall apart after they emerged. Thus we added an example from the time-lapse camera.

Page 16, lines 4-6: Yes I agree that pressure sensor observations could be used to derive calving events, but challenges remain. One challenge is that subglacial hydrological events may cause similar signal as what has described as subaqueous calving in this manuscript.

20 Need justification.

We added a sentence about the challenges with pressure sensors. However, a more detailed analysis of the pressure sensor data is not the scope of this study and will be done in further work.

Page 16, lines 13-15: Perhaps this paragraph needs to be rewritten, because I don’t get the logic of cause and effect. Sentences before and after “Therefore” seem to be out of place.

25 What do tides do with air temperatures and radiation? Other readers may also be confused.

We rewrote this paragraph to make it clear that the surface melt can influence the water level in the crevasses or the glacier dynamics through the subglacial hydrology.

Page 17, Figure 9: In (d) and (e), are the calving events in the deep sector plotted above calving events in the shallow sector? Please note this in the caption, otherwise readers can assume that all these histograms start from 0 in the y-axis.

30

We added the sentence “The calving events in the deep sector are plotted above those in the shallow sector.” to the caption.

Page 17, line 10: Maybe “surface” should be added to the front of “calving event” because subaqueous calving was also discussed?

We added aerial in front of calving event as this is the term used in the rest of the manuscript.

Page 17, lines 13-14: Or it may not have to be explained by other processes? I don't see the necessity of assuming similar ice flux in the two sectors.

5 If the ice flux would be very different for both sectors, we should see this in the flow field and surface characteristics (e.g. crevasses), but higher up the velocities are very similar for both sides of the glacier. We clarified this in the revised manuscript.

Page 18, line 2: Here "center" was used, but at other places "centre" was also used. Please be consistent.

We changed center to centre so that it is consistent in the whole manuscript.

10 Supplement page 1, Figure S1: A more accurate job needs to be done if the front line was estimated visually, because this research studies many relatively small calving events. If there are satellite images at the beginning and the end of the campaign, then they should be plotted here. If no available satellite images at these times, TRI amplitude images can help.

We redid the visualization of the calving front position more accurate.

15 Supplement page 1, Figure S2: As I commented above, please add a panel to show unfiltered water level.

We added a figure with unfiltered water level data in the supplements (Fig S9).

Supplement page 2, Figure S3: I thought the tide data were heavily filtered, why there is a jump around 08:00 on the 20th? Please check.

20 We thank referee 1 for spotting this, the jump is removed in the revised manuscript.

25 **Reply to major concerns Referee 2**

DEM derivation of the glacier front from TRI

The critical part of the paper is the derivation of digital elevation models of the glacier front from terrestrial radar interferometer as developed by Strozzi et al. (2012). However, this method is known to be uncertain, although the large glacier size should help having a greater signal to noise ratio. I think that it is important to extend the paragraph on the error analysis and dedicate a specific figure with a map of the derived DEM(s), statistical distribution of the error in the discussed stable terrain. Assess the uncertainty of the glacier part with the UAV derived DEM too by replacing Figure 3 as the velocity comparison is done in Rohner et al, 2019. I would like to have a Figure showing a study case of the detection and watershed algorithm to assess issues with signal to noise ratio and uncertainty in radar geometry or cartesian coordinates (in the main text or supplementary material).

30

35

We agree with the concern of referee 2 that the error analysis needs more elaboration. We added section 4.1 and Figures S2, S3 and S4, where we investigated the error on stable terrain over time and space. We also compared a stacked TRI DEM with the Arctic DEM.

5 A comparison with the UAV derived DEM to investigate the uncertainty of the glacier part is currently not possible as we do not have a georeferenced UAV DEM for this time period. To do this comparison we would need to georeference it and do a detailed error analysis, which is not part of this paper. Additionally, as we do not have ground control points on the glacier the UAV DEM might be warped in the centre of the glacier.

10 Figure 3 is not meant as a velocity comparison, but the UAV velocity is rather a completion of the TRI-derived velocity data to illustrate the flow field (which we also use to estimate and discuss ice fluxes later in the manuscript).

We add a figure in section 4.1 showing a study case of the calving event detection.

Issues in determining best fit models for calving distribution

15 As seen on Figure 6c and 6d, it is not possible to distinguish between a power law and a log normal models as indicated by a low loglikelihood ratio R between the two distributions and a poor significance value, $p > 0.1$. The only evaluation possible of the power law is a comparison with other heavy-tailed distributions. The conclusion is that the shallow and deep part does not exhibit a transition in distribution from power law to log normal as they cannot be statistically differentiated from each other.
20 Discuss instead whether the distribution over such a short period is representative.

25 With the changed calving event size distribution we find that the shallow sector is following a power law with a p value ≥ 0.1 . For the deep sector both the lognormal and power law models fit well, but none of them fits significantly better. We also agree that the period is rather short to have a representative distribution and we will add a sentence about that. Since we observed a big number of calving events we are convinced that a statistical analysis is meaningful and legitimate.

Ice flux budget: bed topography and missing component

30 The paper bases its analysis on the depth of the fjord but no bed data is provided to support this description (just observations of surfacing rocks). Please use the BedMachine v3 to at least provide an idea of the fjord depth in front of the glacier to the reader. The shallow part may be constituted of two bed pinning points beside a deep valley. Furthermore, simplify the subdivision of the shallow part to only the shallow part regrouping SL, SM and SR.

35 The simple ice flux calculation holds some caveats when identifying a missing volume due to the uncertain fluxgates and filtering of small events. The distribution of these small events may be related to calving mechanisms and ocean melting (undercutting). A more realistic flux can be derived by integrating the ice flux with your surface elevation and velocity data. See my minor comments to improve the understanding of section 5.1.

40 We added the data of BedMachine V3 to the supplement (Fig S8) of the revised manuscript to give an idea about the fjord topography. However, as no direct measurements are available directly at the calving front, the data of BedMachine V3 at the calving front should be considered with care. At and near the calving front the velocity is influenced by additional processes and the estimation of the ice thickness by inferring the surface elevation and velocity data cannot reproduce the bed topography
45 correctly.

We added a more detailed analysis of the ice flux and show it in Figure 7d. We calculated the potential ice flux per bin with our data on velocity and surface height per bin. To include the calving below waterline and the ocean melt we assumed a total ice thickness of 150 m and calculated the flux with this value and the velocity per bin. However, note that these flux estimates are only rough estimates to analyse the rough shares of different calving processes and not exact values of different calving fluxes (but they are consistent with the observed flow fields in Fig. 5). We will keep our subdivision of the calving front as we think it is needed for the interpretation. The three parts of the shallow sector show different characteristics likely due to the bed topography and thus they cannot be seen as one homogenous sector.

10

Better integration of calving wave dataset

The paper should integrate better the ocean wave data as an alternative dataset of calving events (including subaqueous ones?), explain this discrepancy and discuss other potential sources such as iceberg rolling. This better integration of the wave amplitude dataset with the TRI detected calving events would strengthen the discussion and conclusion of the paper.

15

We added a peak detection analysis of the calving wave dataset for a comparison with the TRI detected calving events in Figure 12. However, in this paper we want to focus on the TRI dataset and the established methods. A more detailed analysis of the calving wave dataset is beyond the scope of this paper and the topic of a follow-up paper.

20

Reply to minor comments

25

page 2

Abstract

Please mention that the study is based on derived digital elevation models. Focus on your findings right after your methods instead of following the paper structure: the characteristics of the shallow/deep part (I.5-7), then calving missing calving volume (I.8-10), self-critical system vs less complex model (I.10-11), Calving models vs front geometry (I.11-12) and finally lack of relation to air temperature and tides.

30

We thank referee 2 for the suggestions. We added that the study is done by using digital elevation models. Otherwise we think we already have the suggested structure or did we misunderstand it?

I.2: "in understanding the processes of calving"

35 We adjusted this in the revised manuscript.

I.5 can you find a better word than "source area"? "vertical front area"?

We find source area the more appropriate term as it implies that this is the location where the calving event occurred.

1. Introduction

It is well written and nicely placing the work in its context.

page 3

5

I.12 Add Kohler et al., 2015 in Polar Research [TOCHECK] as they produced the longest calving time series based on seismic records (20 years)

We added Köhler et al. 2016 and we thank referee 2 for the hint.

10

I.14 Delete “can only detect large events” as they can detect small events (even ice falling in a crevasse at the front, Kohler et al., 2019 in The Cryosphere Discussion) when placed close to the glacier front. Their main issue is the volume scaling.

We deleted this part of the sentence.

15

2.1 Study area

I.30 Add that the glacier has been stable and even advanced since 2016 similarly than Jakobshavn Isbrae (based on Planet daily imagery).

Eqip Sermia had a fairly stable front position during the last years with only a small retreat at the southern margin. We added this to the section. We specifically checked satellite images and we cannot see the advance of the front position mentioned by the referee.

20

I. 32 Indicate the time period when 16 m day⁻¹ was obtained: “as measured over our two week period in 2016”? as the 2.5 and 5 m day⁻¹ represents annually averaged velocities, correct?

We included: “...measured over the observation period in 2016...”.

25

page 4

I.1-7 Also present the glacier bed or bathymetry provided in the BedMachine as it covers an area that is now deglaciated (as they use an older surface elevation and glacier mask) and upstream bed geometry is also important to understand the glacier flux at the front.

We added the bathymetry provided in the BedMachine v3 to the supplement (Fig S8) and added a sentence in the study side section.

30

page 4-5

The TRI and environmental data parts are complete and informative.

page 6

3.1 TRI data processing

35

I.15-17 Is the elevation difference just a shift in absolute elevation explained by a difference in geoid or geo-referencing problems of the Arctic DEM or your DEM? Also co-registering the two DEMs before differencing is useful to assess systematic errors outside obvious artefacts.

We added a more complete comparison in the revised manuscript between the Arctic DEM and our DEMs and investigating there the variabilities on stable terrain in more detail. The result is presented in Figure S7. The two DEMs were co-registered before comparing them. The elevation difference is likely not just a shift, it also depends on the slope of the terrain.

5 I.18-19 Please provide a sentence about precision change over time on stable terrain and also ice. You could plot this variability on stable terrain and some upper part of the glacier for the single DEMs and the stacked ones to appreciate the effect of atmospheric disturbances and the improvements from stacking. You could use this variation to provide first order error bars for your volume estimates on Figure 6. In the discussion could you compare your precision to what other studies found.

10 We thank referee 2 for the suggestion, we added a section on the variability between the stacked DEMs on stable terrain over time and space. However, as the glacier area measured with the TRI is highly crevassed and fast flowing, we do not think that an analysis of the variability there is meaningful. We only looked at the variability for the stacked DEMs, however as an example for the watershed algorithm we also included a plot from a non-stacked DEM. We do not think that first order error bars
15 due to the improvements by stacking are meaningful, because it is not only the stacking but also the used threshold which influences the increased signal to noise ratio.

I.20-21 Indicate that the watershed algorithm uses elevation change as source image and merges calving events occurring within 10 minutes due to the stack. Can you define algorithm parameters like the number of start points or maximum points for reproducibility? Please plot an example of your
20 watershed results (here or in supplementary materials) to assess the effect of noise on your segmentation. An error of 10 pixels in radar geometry already causes a volume error of 5625 m³ in range and 12000 m³ in azimuth using 150 m of ice thickness, that is the same order of magnitude than your calving volumes.

We added this information to the method part. Number of start points and maximum points are not
25 needed for the algorithm. The only needed parameters are a maximum and minimum value, which are used for the markers in the algorithm. The minimum value is 5 m as we define this as background, while for the maximum value we used 15 m. We added the maximum value to the methods part. We added an example of the watershed results to section 4.1.

I.23-24 “10 pixels **in area**” Specify that in the context of your grid asymmetry, your area filter is more
30 likely to remove events that are long instead of wide, thus you apply this second filter of 3 pixels. Add that 3 pixels is equal to 11.25 metres.

We added this information to the manuscript.

I.24 “When applying [...] are removed”. The noise observed on stable terrain is not removed, but the
35 signal to noise ratio is higher for the filtered events. Moreover, quantify the number or area of excluded events or give a percentage.

We changed that sentence to: “When applying these filtering thresholds, the signal to noise ratio is higher on stable terrain than for the non-filtered events.” We added a percentage of excluded events to section 4.1.

I.20-24 How do you deal with the zero elevation or water elevation when calving occurs along the entire ice column (i.e. column collapse)? Parts of the DEM covering the sea may have Not A Number values or problems with icebergs?

5 The water elevation is set to 0 also where there are Not A Number values. Thus, it does not influence the calculation if calving occurs along the entire column. The calving at Eqip Sermia happens mostly through ice avalanches, not resulting in big icebergs. Bigger icebergs remove the ice melange in front of the glacier, which results in a loss of coherence. Due to this loss of coherence the area including the iceberg is not included in the analysis. Icebergs further away are not included anymore as they are not within the glacier front mask.

10 *page 7*

I.4-6 Rephrase the last line that explains what a “good” p value is and means. Specify that the maximum-likelihood methods are used because of the non-linearity of the fitted curve and that one implication is that the resulting log-likelihood is a relative score of how good two fitted models perform against each other instead of “an absolute score”.

15 We added this information to the manuscript and changed the last line according to referee 1.

I.8 Add that 120 interferograms is approximately 2 hours.

We added this information to the manuscript.

20 I.7-10 Indicate the theoretical maximum velocity that the TRI measures with an interval of one minute (it should be of the order of 6 metre per day) as this will be useful to explain the differences with the UAV velocity data. [TAZIO equation]

We did not add this information as the UAV velocity data is not meant for comparison but only as an additional information (for example for the flux estimation) due to the limited area of the TRI velocity field.

3.2 Pressure sensor data processing

25 I.15 Indicate the frequency of the low pass filter or used methods.

We added the pass frequency of the low pass filter, which is the same as for the high pass filter.

4. Results

30 The key result of the paper is the TRI-derived DEMs but the velocity (4.1) is presented first instead. Add text and figure(s) specifically on the generated DEMs and signal improvement by stacking before section 4.2 on calving detection results or a comparison with the UAV DEM.

We added a section about the derived TRI DEMs and the variations before the velocities as section 4.1.

4.2 Magnitude and source of area of calving events

Abandon the subclassification of the shallow sector as it confuses the results

We will keep the subclassification as the three parts of the shallow part are not homogenous.

I.25 I suggest a simpler section title: Area and location of calving events?

We thank referee 2 for this suggestion. However, we think area is misleading as it is more the size of the events which is discussed here.

- 5 I.29 Add the number of filtered/removed events for each sector as the filter may affect the number of calving events. I have a hunch that the deeper sector may have more small events, likely filtered out, due to the effect of higher submarine frontal ablation.

We added the sentences: "Comparing the amount of extracted events for a threshold of 1 m and of 5 m shows that with the threshold of 5 m 77% less events were extracted for both, the deep and the shallow sectors. The usage of the shape condition for events smaller than 40 pixels leads to 49% less events for the shallow and 54% less events for the deep sector." to section 4.1.

page 8

I.1 Replace "frequencies" by "number"

We changed that accordingly.

- 15 I.2 "**four** orders of magnitude".

We thank referee 2 for spotting this. We changed it in the manuscript.

I.2 Use the same order of magnitude i.e. 10^3 for easier comparison, too.

We changed the numbers to the same order of magnitude.

- 20 I.2 I do not understand how you get a minimum volume of 160 m³. If you take a minimum area of 10 pixels with 30 m² per pixel, you get a height of 0.53 m. This does not match your vertical change threshold of 5 m. So, I guess the comma is misplaced, it must be 1.6 10^3 m and you were correct with "three orders of magnitude".

$Volume / (10 \times Pixel\ Area) = Height$ or $160 / (10 \times 3.75 \times 8) = 0.53$.

- 25 We thank the referees for spotting this. We realized that some of the events were considered as calving events even if they are collapsing seracs upstream the glacier. They were included as they were located exactly on the border of our glacier front mask. Those events are excluded in the revised manuscript.

The algorithm takes also events into account where pixels of less than 5 m decrease are surrounded by pixels of more than 5 m decrease. Thus the events can be smaller than the calculated minimum size of a calving event.

- 30 I.8-11 Delete the subdivision of the shallow sector it does not bring much to the comprehension of the calving distribution. Or just keep the rock part: M.

We will keep the subdivision as the shallow sector is not homogenous. Sector SM has less events than the other two sectors, which is likely caused by differences in the bed topography.

page 9

5 Table 1: Could this table be combined with Figure 6a and 6b by placing a text in the corner or a horizontal boxplot at the top? Rarely calving distribution are presented as a table, making it difficult to compare with other studies.

We understand the concerns of referee 2, but also other studies used a table and we find it clearer like this.

page 11

10 I.19-21 Develop the detail of your computation (numbers?) and how you obtain 25% in the text and on Figure 5d.

We exchanged the right axis of Figure 7d and provide now calculated ice fluxes over the front. The calculation on the percent are done in the text.

4.3 Calving statistics

15 I.23 Describe first what you want to achieve, meaning model the calving distribution with non-linear fitting models to assess whether you observe a “self organised critical system”.

We added the sentence: “The calving distribution was compared with non-linear fitting models to investigate if a self-organised critical system can be observed.”

20 I.27-31 It is not clear to me what is the basis for selecting a log-normal against a power-law in both sectors as the results of the maximum likelihood (and visual inspection) show that the fitting models are as good and with similar parameters.

Due to the new condition used in the filtering of calving events, the event size distribution changed. The shallow sector follows now a log-normal model with a p value = 0.1, while for the deep sector both a power law and a log-normal model fit, but none significantly better.

page 12

25 4.4 Pressure sensor records

In order to find the missing component presented in the discussion, it would really help to derive a rough calving catalogue based on a peak detector or even manual picking and neglecting other sources of wave oscillations such as iceberg rotation.

30 We added the detected peaks of the pressure sensor data to Figure 12. Thus a comparison with the TRI derived calving events becomes possible.

5. Discussion

I.14-15 “[...] no clear temporal pattern of tidal or diurnal recurrence [...]” comes to me as a surprise as it is not presented in the results (but should be, including Figure 9).

We deleted this part of the sentence here as it comes later in the discussion.

5.1 Relation to ice flux and other processes

I.16 Which “other processes”? Be specific. Here you want to close the “ice flux budget at the calving front” or find the “Missing volume in the deep sector”

We changed the subtitle to “Relation to ice flux”.

5 I.17-23 Your simplification to compute the ice flux is fair but neglects variations in ice thickness and important processes such as submarine melt. It is thus not convincing that the total calving volume matches the computed flux. Try to obtain the ice flux by integrating the glacier velocity, height for aerial calving (ice thickness would be better assuming a certain bed topography) and the glacier discrete width (for each space unit) maybe even upstream of the front assuming constant front.

10 We added to Figure 7 an ice flux estimate along the front derived from the available velocity and surface height data. Additionally, we produced an ice flux estimate that uses a constant front thickness of 150 m to also account for the ice flux underwater. We assume that the front thickness is similar for both sections as we cannot see changes in surface characteristics (e.g. crevasses) on the surface of the glacier.

15 *page 14*

I.1-6 I am confused here as you seem to compute the aerial ice flux using the ice height above water (150 m) and thus the missing aerial volume in the deep sector cannot be directly caused by oceanic melting, but indirect effect of the undercutting and thereby lower stress threshold for breakoff. Compare the volume you detect with the aerial ice flux in the deep sector with an ice height of 50 m. The
20 estimated volume from the ice flux is then threefold lower than your previous estimate and is closer to your TRI calving volume estimate.

The 150 m is not used to calculate the aerial ice flux but the total ice flux (with subaquatic ice flux). So in Figure 7d we calculated now the ice flux with the available front height and additionally with an ice thickness of 150 m to represent the total ice flux.

25 I.3-4 Before neglecting the role of filtered calving events in explaining the missing volume, could you check that the number of filtered calving events is proportionally the same in the shallow and deep sector assuming a homogeneous noise along the front? The effect of oceanic ice melt and undercutting in the deep sector may cause smaller blocks to fall at lower stress threshold than in the shallow part. This is coherent with your observation that few large calving events occur in the deep
30 part.

We added a discussion part about the calving of small volumes at the end of this section.

I.8-15 Good discussion and comparison. I would just add the year when the oceanic melt was obtained as it depends on warm Atlantic water intrusion that has reached a peak in 2007 and has weakened since (hence the glacier advances in the region).

35 We added that the summer melt rates that were measured in 2008.

I.15 “the contact area [...] is much smaller” by how much?

We added the water depth of the shallow sector as a reminder.

I.20 Indicate that the 75% mass removal in the deep sector occurs only over two third of the calving front, showing a greater efficiency of melting in the submarine part of the front.

We deleted this number as we do not know how much is actually explained by the subaquatic mass loss and how much with small calving events.

5 5.2 Influence from cliff height and shape

Overall, the discussion is good, but there is no discussion on the effect of undercutting on stress regime (see comments in 5.1).

We added this to the chapter before to the section with calving of small events.

I.22 Alternative title: “Effect of steeper and higher ice cliff ” or “Role of front geometry on stress

- 10 We thank referee 2 for this suggestion. However, in this section not only the cliff height and steepness but also the front shape including the rock ridge is discussed.

page 15

I.1 “decreasing water level” do you mean tides or specify what causes water level to decrease in crevasses.

- 15 Here we mean not that the process of decreasing water level causes the crevasses further upstream. The water level in front of the glacier influences where the crevasses open. If the water level is small then the crevasses open higher upstream. We rephrased it and hope it is clearer now.

I.3-7 Nice interpretation that could also be applied to the deep sector. You can verify your hypothesis by comparing front positions and the glacier retreat seen in Figure S.1 may be significant.

- 20 Thank you for the suggestion. We agree that in the deep sector undercutting due to oceanic melt may lead to small calving events, which cannot be detected with the TRI. We moved this section to the chapter before and added the undercutting due to oceanic melt at the deep sector.

5.3 Calving statistics

- 25 Although the discussion is well written and nicely supported with recent studies, the low p values of the likelihood test on Figure 6 show me that both a power law and log-normal can explain your distribution in both sectors. Thus reformulate your question here as the power law distribution can also be attributed to the shallow sector.

Due to the new filtering condition the statistics changed and we updated this section.

- 30 I.8 Alternative title: “Self-organised critical system vs less complex systems” or “calving distribution and driving mechanisms” or “calving distribution”

We changed the title to “Calving event size distribution”.

- 35 I.12-13 All cited studies estimate aerial calving and neglects subaqueous events. The main reason for a too steep power law curve may be that the study period is too short and there were too many (or not enough) calving events larger than 10^5 m³ (or between 10^4 and 10^5 m³). This would also explain the misfit on Figure 6c.

We thank referee 2 for this hint but we had to change this paragraph due to the new results.

I.16 “[...] instability with **many small** events [...] events of **greater** magnitude”

We had to delete this sentence in the revised manuscript.

I.17-18 I do not understand the point of that sentence. Rephrase or delete.

5 We deleted this sentence.

5.4 Comparison with pressure sensor data

Discuss whether you can identify waves of rolling iceberg from those of calving events. Subaqueous events can often be confused with icebergs rolling close to the glacier front as we can often only identify them from the produced waves.

10 We added a sentence about the challenges of analysis wave data at the end of the section. A more detailed analysis of the pressure sensor data will be done in a follow up study.

I.25 Alternative title: “Comparison with calving wave signal”

page 16

5.5 Relation to external forcing

15 The air humidity is not present here (section 2.3) and would be useful to assess potential precipitation periods and atmospheric disturbance on the radar signal. Precipitation tends to mess up surface melt and tidal signals seen in calving event occurrence. The temporal resolution used in Figure 9 for your calving events may be too high to find a relation that often occurs on hourly time scale. On Figure 9d-e, resample your calving data and apply a cutoff for the two-three largest events around 0.2 in 9d and 10
20 in 9e. The legend can be plotted once in between the two panels.

We could not find a relation with the air humidity. Also Eqip Sermia is a very dry place with not a lot of precipitation. Thus we did not add the air humidity. We could not find a different pattern by using hourly timescale. We kept the higher temporal resolution as we would lose information by lowering the resolution. We added a cut-off to the high values and plotted the legend only once.

25 I.12 Alternative title “Absence of meteorological and tide effect”

We thank referee 2 for this suggestion. However, we think that we have not enough data to ensure that the meteorological and tide effect is absent.

I.14-15 The sentence on surface melt is not coherent with the sentence before that finishes on tide effects.

30 We changed that part and hope it is now clearer.

page 17

6. Conclusion

Update the conclusion after answering my comments.

I.10 “We developed a novel **detection** method **based on TRI DEM differencing** to establish [...]”

We changed that sentence in the revised manuscript.

---- Figures ----

5

Figure 3

Remove the velocity comparison as a more thorough comparison is achieved in Rohner et al, 2019 (refer to their Figures). Instead show here a plot of the mean velocity for the entire period and beside or in another figure plot a comparison of the TRI DEM and Arctic DEM including a distribution of their difference (or do you have the UAV derived DEM as well?). Eventually, in a new figure plot the DEM before and after one selected calving event, the subtraction of the DEMs, mask of the glacier front and the watershed result. Condense the caption: “Velocity field at the glacier front measured a) with the TRI on 19 August 2016 and b) with a UAV”

10

15

Fig 5 in revised version: The velocity of the UAV is not meant as a comparison but to get an idea of the velocity field over a larger area (e.g. for ice flux estimates) as the TRI velocity field is only available at the front. We added a plot of a TRI derived DEM, a comparison between TRI DEM and Arctic DEM (supplement), a differentiated DEM (unstacked and stacked) and the watershed result. We condensed the caption.

Figure 4

20

Plot the rough location and view angle of the picture

Fig 6 in revised version: We plotted the location and view angle of the picture roughly.

Figure 5

Panel a

25

Could you use an image taken from the TRI position or the radar image in Figure 4 cropped and rotated to fit the format here and with the line you use to stack your data in c)? The current image is confusing as it is in a different orientation than the TRI (taken from a hike to front, I guess) and saturated (I cannot see the front texture).

Fig 7 in revised version: We exchanged the image with an image taken close to the radar position but further away.

30

Panel b-d

extend the plot to the end of the right plot margin. If this was for the legend in b, change min max lines to a polygon (shadow) and place the legend horizontal at the bottom of the panel such as --- Elevation --- Mean velocity [grey box] Min/max velocity. Indicate the location of the sectors above panel b) and delete them from panel c).

35

Fig 7 in revised version: The plot does not go to the end of the margin to make it comparable with the image in panel b which is slightly wider.

Panel c

Please use a linear colour scale. Your current palette highlights mostly areas with no calving volume change and the yellow parts of your spectrum (7000 m³) and a bit the red ones. Choose a linear colour scale from light yellow to red or blue. Write "data gap" between 22 and 23 Aug.

- 5 Fig 7 in revised version: We changed the colours here, no calving is now grey which makes the calving events better visible. We wrote data gap in the caption.

Panel d

- 10 Delete the red dashed line representing 50% and 100% of the mean calving volume in the shallow sectors. I don't understand which message it is supposed to convey. Do you mean that 50% is equal to ~0.4 106 m³ of calving volume?

Fig 7 in revised version: We deleted this and added the ice flux to this graph.

Figure 9

- 15 Stretch the vertical axis for all panels to highlight the variations of your parameters. Shift the shortwave data so that we see that the curve goes to zero during the night (there must still be some light at this latitude mid-august?). Use the same temporal resolution for the Volume and number of events than the two first panel for instance hourly. Cutoff the extreme value on the 26 Aug. evening and write its value on the figure with an arrow pointing to the top. (also see comments *page 16*)

- 20 Fig 12 in revised version: We changed the y-axis to make the variations better visible. The shortwave data is now shifted. We cut-off the extreme values and added arrows pointing to the top. We did not change the temporal resolution as we do not see a different result with a lower resolution and we would lose information in doing so.

Calving event size measurements and statistics of Equip Sermia, Greenland, from terrestrial radar interferometry

Andrea Walter^{1,2}, Martin P. Lüthi¹, Andreas Vieli¹

¹Institute of Geography, University of Zurich, Zurich, Switzerland

5 ²Laboratory of Hydraulics, Hydrology and Glaciology, ETH Zurich, Zurich, Switzerland

Correspondence to: Andrea Walter (andrea.walter@geo.uzh.ch)

Abstract. Calving is a crucial process for the recently observed dynamic mass loss changes of the Greenland ice sheet. Despite its importance for global sea level change, major limitations in understanding the [process of calving](#) ~~process~~ remain. This study presents [high resolution](#) calving event data and statistics recorded with a terrestrial radar interferometer at the front of Equip Sermia, a marine terminating outlet glacier in Greenland. The [derived digital elevation models](#) ~~data~~ with a spatial resolution of several meters recorded at one-minute intervals ~~were was~~ processed to provide source areas and volumes of ~~9061700~~ individual calving events during a 6 day period. The calving front can be divided into sectors ending in shallow and deep water with different calving statistics and styles. For the shallow sector, characterised by an inclined and very high front, calving events are more frequent and larger than for the vertical ice cliff of the deep sector. We suggest that the calving volume [deficiency of 90% missing](#) in our observations of the deep sector is removed by oceanic melt, ~~and~~ subaqueous calving [and small aerial calving events](#). ~~Assuming a similar ice thickness for both sectors~~ [which](#) implies that subaqueous mass loss must be substantial for this sector with a contribution of up to ~~675~~ % to the frontal mass loss. The size distribution of the ~~shallow~~ ~~deep~~ sector [is represented by a log-normal model](#). ~~follows a power law~~, while ~~for the deep~~ ~~shallow~~ sector [the log-normal and power-law model fit well, but none of them is significantly better](#). ~~is likely represented by a log-normal model~~. Variations in calving activity and style ~~between~~ [within](#) the sectors seem to be controlled by the bed topography and the front geometry. Within the short observation period no ~~simple~~ ~~clear~~ relationship between environmental forcings and calving frequency or event volume could be detected.

1 Introduction

Over the past decade rapid retreat, thinning and flow acceleration of many outlet glaciers contributed substantially to the observed increasing mass loss of the Greenland ice sheet (Moon et al., 2012; Enderlin et al., 2014; King et al., 2018) and consequently to global sea level rise (Rignot et al., 2011; IPCC, 2014). These dynamic changes seem to be related to a general warming ~~trend~~ of air temperature and water masses [around](#) ~~in~~ Greenland (Straneo et al., 2013). Several studies have shown a high sensitivity of outlet glaciers to environmental forcings (Holland et al., 2008; Howat et al., 2010; Carr et al., 2017), while the fjord topography is an important control for the dynamic behaviour of the outlet glaciers (Warren, 1991; Catania et al., 2018). However, major limitations in understanding and predicting the dynamics of outlet glaciers [remain, e.g. a complex link between atmospheric forcing and calving activity and insufficient resolution in models and observations](#). ~~remain and~~ The detailed relationship between climate and dynamic changes is still poorly understood (McFadden et al., 2011; Vieli and Nick, 2011; Straneo et al., 2013).

Calving is a crucial process [for the dynamic behaviour of](#) ~~controlling how~~ tidewater glaciers, [but the detailed mechanisms and relation to environmental forcing are not well understood](#). ~~react to changes in environmental conditions~~ (Joughin et al. 2004; Thomas, 2004; Nick et al., 2009). Calving rates ~~are~~ ~~are controlled by~~ [generally a function of](#) the stress state at the terminus. When stresses exceed the strength of the ice, fractures ~~can~~ form and propagate, [until blocks of ice separate](#) ~~and a lead to the block of ice can break off of ice~~ from the front. Mechanisms causing fractures to propagate are: 1) spatial gradients in the

glacier velocity, 2) changes in frontal geometry (front position, height), 3) undercutting of the glacier front by melting at or below the water line and 4) buoyancy forces (Pralong and Funk, 2005; Benn et al., 2007). Direct and continuous observations of the calving process are difficult and therefore the underlying mechanisms are observationally under-constrained. Most existing studies investigated the calving process on longer time scales by considering time averaged calving rates or fluxes. Available studies on individual calving events focus mostly on discontinuous (Warren et al., 1995; O'Neel et al., 2003) or indirect measurements (O'Neel et al., 2010; Walter et al., 2010; Bartholomaus et al., 2012; Glowacki et al., 2015). Several studies investigating the process of ice break-off over short time scales show that the process of calving has a very high temporal and spatial variability and that the observed calving size distribution for grounded tidewater glaciers is following a power law (Chapuis and Tetzlaff, 2014; Åström et al., 2014; Pętllicki and Kinnard, 2016). However, these investigations focus mostly on time averaged estimates of volumes, discontinuous datasets, indirect measurements or a combination thereof and thus lack continuous direct observations of the calving event size. For an accurate representation of the calving process in current flow models and to link calving activity with potential environmental forcings more detailed observations with high temporal and spatial resolution are necessary.

During the last 20 years observational data for monitoring calving glaciers ~~were was~~ mainly obtained through satellites at a sampling frequency that is not suitable to observe individual calving events. Other more in-situ based approaches such as terrestrial photogrammetry using time-lapse cameras (dependent on weather and daylight) (Vallot et al., 2019) and drone data (limited temporal resolution) (Jouvet et al., 2017) also show severe limitations regarding the observation of the highly variable calving process. Promising results were obtained with seismic monitoring of calving (Amundson et al., 2012; Walter et al., 2013; Bartholomaus et al., 2015, Köhler et al., 2016, Köhler et al., 2019) and maximum wave amplitudes as a proxy for calving fluxes (Minowa et al., 2018), but those methods ~~can detect only large events and~~ cannot quantify calving event volumes directly. Terrestrial laser scanning allows to measure the volume of individual calving events (Pętllicki and Kinnard, 2016), but requires suitable meteorological conditions and lacks the temporal resolution to detect individual calving events. Terrestrial radar interferometers can overcome most of the mentioned limitations and have been used to study the effects of tidal forcing on the front of an outlet glacier (Voytenko et al., 2015), to investigate calving rate and velocity (Rolstad and Norland, 2009), to determine calving event frequency (Chapuis et al., 2010), velocity variations and grounding line motion (Xie et al., 2018), pro-glacial mélange thickness (Xie et al., 2019), glacier's response to calving (Cassotto et al., 2018) or to estimate the volume of a single large calving event (Lüthi and Vieli, 2016).

This study aims at investigating the calving process and event statistics by using a terrestrial radar interferometer (TRI). For this purpose the calving front of the tidewater outlet glacier Eqip Sermia in Greenland was investigated with a TRI at one-minute intervals during a 6-day field campaign in 2016 ~~and with a spatial resolution of several meters~~. The resulting high resolution time-series of individual calving event volumes and related source areas allow us to investigate the relationship between calving front geometry, calving flux and environmental forcings such as tides or air temperature.

2 Study area and data acquisition methods

2.1 Study area

Eqip Sermia (69°47'N, 50°15'W) is an ocean terminating outlet glacier located at the western margin of the Greenland ice sheet. Observations of the glacier front position, surface elevation and flow speed are available at ~~almost~~ decadal resolution since 1912 and show a doubling of discharge and accelerated retreat within the last two decades (Lüthi et al., 2016). Between 1912 and 2006 velocities between 2.5 and 5 m ~~day~~⁻¹ were observed, whereas today the glacier front velocities measured over the observation period in 2016 are reaching up to 16 m ~~day~~⁻¹. After a rapid retreat starting in 2010, the calving front position stabilized during the last five years.

The calving front has a width of 3.2 km and a height above the water line between 50 and 170 m. The ~~whole-entire~~ front is grounded but the water depth in the northern half is very shallow (0 – 20 m, termed 'shallow sector' from now on) and locally the bedrock protrudes above the water. In the southern sector the water depth is 70 to 100 m (~~termed~~ subsequently termed 'deep sector' ~~from now on~~). Directly at the calving front no depth sounding data are available and the given depth estimates are extrapolated from bathymetric surveys in the proximity of the current front position (Rignot et al., 2015; Lüthi et al., 2016). The difference in bed topography between the deep section and the shallow section is also visible in the bathymetry from BedMachine v3 (Fig. S8; Morlighem et al., 2017). Related to the contrast in water depth, the geometry of the front is ~~also~~ distinctly different between the two frontal sectors. In the deep southern sector the front is vertical and the frontal cliff height lower than in the shallow northern sector where the front is inclined (Figs. 1 and 2).



Figure 1: Overview of Eqip Sermia and measurement sites. The positions of the terrestrial radar interferometer (TRI), the pressure sensor (PS) and the two weather stations (AWS) are indicated by triangles. The deep and shallow calving front sectors are marked with red and blue lines. Background: Sentinel-2A scene from 3 August 2016 (from ESA Copernicus Science Hub: <https://scihub.copernicus.eu>).

2.2 Terrestrial radar interferometer

A terrestrial radar interferometer (TRI, Gamma GPRI) was installed on bedrock 150 m above sea level across the bay of Eqip Sermia at 4.5 km distance (69.7523 N / 50.2520 W; Figs. 1, 2) with the line-of-sight in flow direction of the glacier. The measurements were repeated at one-minute intervals from 19 August 2016, 18:40 UTC to 27 August 2016, 10:30 UTC. This allowed us to produce an almost continuous record of velocity and elevation change over 7.65 days with a 1.53 days break (22 August 2016, 00:55 UTC to 23 August 2016, 13:00 UTC) due to an instrument failure.

The Gamma GPRI is a real-aperture radar interferometer featuring one transmitting and two receiving antennas. Acquisitions are obtained by antenna rotation along the vertical on a precision astronomical mount. Consecutive interferograms from one of the receiving antennas are used to calculate the velocity. The two receiving antennas facilitate reconstruction of the topography. The radar interferometer operates at a wavelength of $\lambda = 17.4$ mm (Ku-Band, 17.2 GHz). The range resolution is approximately 0.75 m, while the azimuth resolution is 0.1 degrees corresponding to 7 m at a slant range of 4.5 km (Werner et al., 2008a).

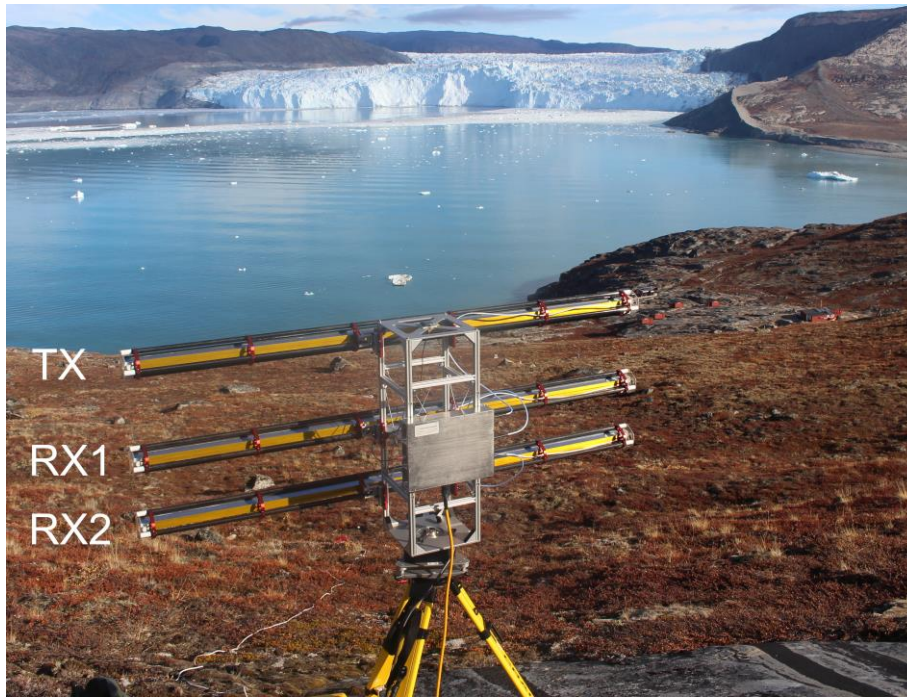


Figure 2: The terrestrial radar interferometer (TRI) located opposite of the front of Eqip Sermia at a distance of 4.5 km (image: M. P. Lüthi, 2016). The TRI has one transmitting (TX) and two receiving antennas (RX1, RX2).

5

2.3 Environmental data

Two automatic weather stations (AWS) with Decagon Em50 data loggers were installed at the sites indicated in Figure 1 and collected data in one hour intervals during the entire whole field campaign. AWS2 located next to the ice edge at 362 m a.s.l. (69.79442 N / 50.16115 W) measured air temperature and relative humidity (VP-3 hHumidity tTemperature and vVapor pPressure sSensor) and wind (DS-2 sSonic aAnemometer). AWS1 near the TRI at 60 m a.s.l. (69.75556 N / 50.25301 W) measured additionally incoming shortwave radiation (PYR sSolar rRadiation sSensor) and precipitation (ECRN-100 hHigh-Resolution rRain gGauge). The meteorological conditions at the ice edge (AWS2) are influenced by the ice sheet while at AWS1 next to the TRI it is more representative for the weather elimate conditions at the shore of the fjord.

15 Tides and waves induced by calving were recorded in the fjord with a RBRsolo pressure sensor (PS; Fig. 1) at a sampling rate of two seconds. The pressure sensor was installed at the shore at a distance of 4.5 km from the ice front (69.75731 N / 50.26490 W, Fig.1). To protect the sensor from floating ice and moving rocks it was fixed in a metal pipe that was attached to a rock at the shore by a steel cable.

3 Data processing methods

3.1 TRI data processing

The GPRI transmits the radar signal from antenna TX and records it by the two receiver antennas RX1 and RX2, which enables spatial interferometry (Fig. 2). To reconstruct topography, interferograms were produced using a standard workflow following Caduff et al. (2015) using the Gamma software stack. The resulting interferograms were unwrapped, using stable features on bedrock as reference. Following Strozzi et al. (2012), the unwrapped phases were then converted to topography z :

$$z = \frac{\lambda}{2\pi} \frac{R}{B} \phi + \frac{B}{2} - \left(\frac{\lambda}{2\pi}\right)^2 \frac{\phi^2}{2B},$$

where $\lambda = 17.4$ mm is the wavelength, R the range to a point on the ground, $B = 0.25$ m the baseline between the two receiving antennas, and ϕ the measured interferometric phase. [To correct for systematic error sources, which can be caused by errors in the reference heights and instrumental geometry, baseline errors and errors caused by a not perfectly vertical mounting of the three antennas \(Strozzi et al., 2012\), a correction factor was calculated. This was done by comparing the calculated DEMs with the Arctic DEM and choosing control points on stable terrain at different distances from the radar. The resulting correction factor was multiplied with the calculated topography to minimize absolute uncertainty in the height estimates.](#) To reduce noise from atmospheric disturbances 10 [consecutive](#) elevation models were stacked. This noise is mainly due to phase shifts in the interferogram induced through changes in air pressure, temperature and humidity (Goldstein, 1995). The final elevation models have a resolution of 3.75 m in range and about 8 m in azimuth direction at the glacier front and were obtained at 10 min intervals over the whole campaign.

The accuracy of the so obtained DEMs was evaluated by comparing ~~son of them on stable terrain~~ with [the Arctic DEM \(Porter et al., 2018\) as a reference DEM on stable terrain.](#) ~~We chose the Arctic DEM (Porter et al., 2018) which on stable terrain outside the glacier yielded elevation differences around 5 m in flat areas and differences up to 10 m in steep areas.~~ The variability between the calculated TRI elevation models on stable terrain was investigated by [looking at the DEM differences over time and space.](#) ~~randomly choosing 30 values resulting in a mean variability of 1 m and a maximum variability of 5 m.~~

In a next step consecutive stacked elevation models were subtracted. The negative height changes at the glacier front were ~~identified~~ [interpreted](#) as calving events. [Due to the stacking, calving events within 10 minutes are merged together.](#) The aerial extent of individual calving events were extracted [from the calculated height changes](#) with the watershed segmentation method from scikit-image (van der Walt et al., 2014) with a height change of [15 m as starting points for the calving events and 5 m](#) as threshold. This threshold corresponds to the maximum variability of the height between elevation models on stable terrain outside the glacier. Height changes of less than 5 m are considered as noise and filtered out. Additionally, calving events smaller than 10 [adjacent](#) pixels and with a [bounding box](#) width smaller than 3 pixels ([11.25 m](#)) were excluded as noise. [Thus, only calving events with both, > 10 adjacent pixels and a bounding box width larger than 3 pixels, were extracted. Due to the asymmetric grid, events extended in range direction are more likely to be filtered out with the 10 pixel filter than wide ones. As noise has mostly an irregular shape, calving events smaller than 40 pixels also needed to fulfil the condition \(number of](#)

[pixels x 1.6](#) \geq (number of pixels in bounding box). This condition is subsequently termed [shape condition](#). When applying these filtering thresholds, the ~~height changes~~[signal to noise ratio is higher](#) on stable terrain [than for the non-filtered events](#) ~~are mostly removed~~. To exclude volume changes from collapsing seracs in the highly crevassed ice [surface](#) further upstream a mask around the glacier front was used. The mask is defined as a line along the front with a buffer of 20 pixels (approximately

5 75 m) on each side of the line ([Fig. 4](#)). All height changes outside the mask were ignored in the data processing.

For visualization the radar image pixels were mapped into cartesian coordinates. Since resampling is a possible source of error, all calculations were performed in the radar geometry and only the final results were georeferenced. Nearest neighbour interpolation was used to resample the radar data to the cartesian UTM22N grid.

Next, we investigated whether the calving event sizes follow a size-frequency distribution. To test whether the measured

10 calving volumes V are explained by an exponential ($e^{-\beta V}$), a log-normal ($\frac{1}{V} \exp[-\frac{(\ln V - \mu)^2}{2\sigma^2}]$) or a power-law ($V^{-\alpha}$) size frequency distribution a statistical analysis using the Python package `powerlaw` was applied (Alstott et al., 2014). The package uses maximum-likelihood methods (Clauset et al., 2009) [due to the non-linearity of the fitted curve](#) and gives as result the log-likelihood ratio R , which is used to investigate which model fits the data better [on as a relative score](#), and the probability value p , which tells if one can trust the sign of R [\(when \$p \geq 0.1\$ \)](#) ~~and should be $p \geq 0.1$~~ .

15 Ice flow velocities were calculated from consecutive interferograms of TRI acquisitions in one-minute intervals. To reduce noise, 120 interferograms ([2 hours](#)) were stacked before phase unwrapping with respect to a reflector on stable terrain. The unwrapped phases can then be converted into line-of-sight displacement $\delta = \frac{-\lambda\phi}{4\pi}$ (Werner et al., 2008b), with a displacement measurement sensitivity smaller than 1 mm.

3.2 Pressure sensor data processing

20 The pressure sensor (PS; Fig.1) recorded the water pressure in the fjord opposite of the calving front, which can then be converted to water height and thus the amplitudes of the tides and calving waves are known. A high-pass filter with a pass frequency of 0.001 Hz was used to extract the calving waves which were then compared with the calving events detected by the TRI. [The peaks of the calving waves were detected by using the peak detection algorithm detect peaks \(Duarte and Watanabe, 2018\)](#). Similarly, ~~t~~he tides were extracted with a low-pass filter [with a pass frequency of 0.001 Hz](#) and are

25 compared with the extracted calving events in order to identify a potential relationship between the tides and the calving events.

4 Results

[4.1 DEM generation and calving event extraction](#)

[A DEM calculated with the TRI data and stacked over 60 minutes is presented in Figure 3. The elevation above sea level is with 50 to 90 m lower on the southern side of the glacier, while at the northern side the elevation reaches up to 170 m.](#)

- To assess their uncertainty, the DEMs were compared to the Arctic DEM (Fig. S7). This comparison shows that on stable terrain, marked with a yellow box, the difference is around 5 m in flat areas, while it reaches about 15 m in steeper areas. The variability between the TRI derived DEMs was investigated over time and space for the stable area marked in Figure 3. The mean height difference between the consecutive TRI derived DEMs is between 1 and 2 m. The mean height difference as well as the standard deviation increases with distance and is higher in steeper areas (Fig. S2). The mean height difference of the stable terrain shows no clear trend over time (Figs. S3 and S4).
- The calving events were extracted by using the height changes of the consecutive TRI derived DEMs. In Figure 4 an example of unstacked height differences, of stacked height differences and of the finally extracted calving event is given in radar geometry. It is clearly visible that the stacking improves the quality of the height difference map. The same calving event is also traceable on the raw radar images as it generated waves (Fig. S5). The filtering methods used for the extraction of calving events reduce the number of calving events but also increase the signal-to-noise ratio. Comparing the amount of extracted events for a threshold of 1 m and of 5 m shows that with the threshold of 5 m 77% less events were extracted for both, the deep and the shallow sectors. The usage of the shape condition for events smaller than 40 pixels leads to 49% less events for the shallow and 54% less events for the deep sector.
- To assess the distribution of the noise along the front, positive height changes were calculated using a minimum size of 10 pixels, a width of 3 pixels and the shape condition for all events (Fig. S6). The result shows that the shallow sector is likely more influenced by noise than the deep sector even after filtering. However, looking at unstacked and stacked height changes (Fig. 4) and the mean variabilities of the differentiated DEMs, the signal-to-noise ratio in the shallow sector was increased considerably.

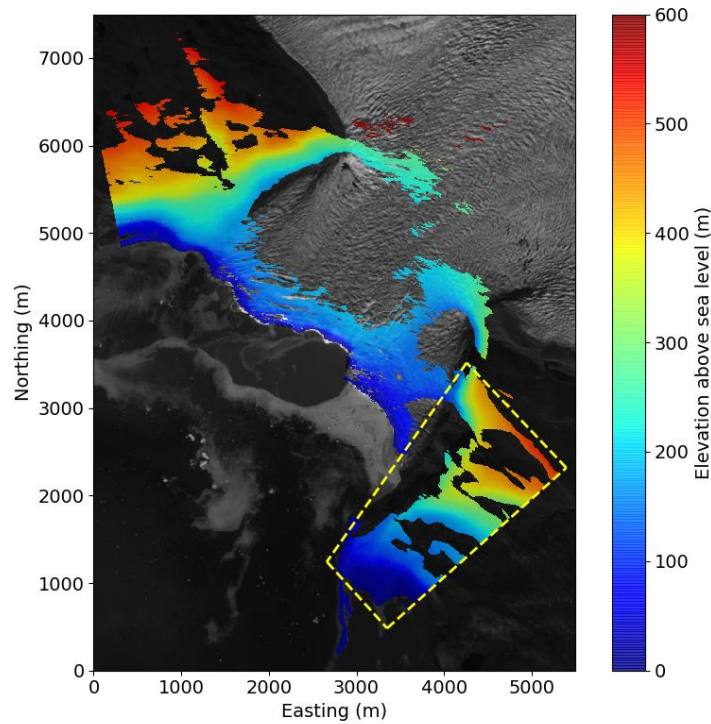


Figure 3: TRI derived DEM stacked over 60 minutes. The yellow square marks the stable terrain area where the mean variability was investigated (see also Fig. 4). The origin of the coordinate system corresponds to 527350° E / 7739550° N (UTM 22N). Background: Sentinel-2A scene from 3 August 2016 (from ESA Copernicus Science Hub: <https://scihub.copernicus.eu>).

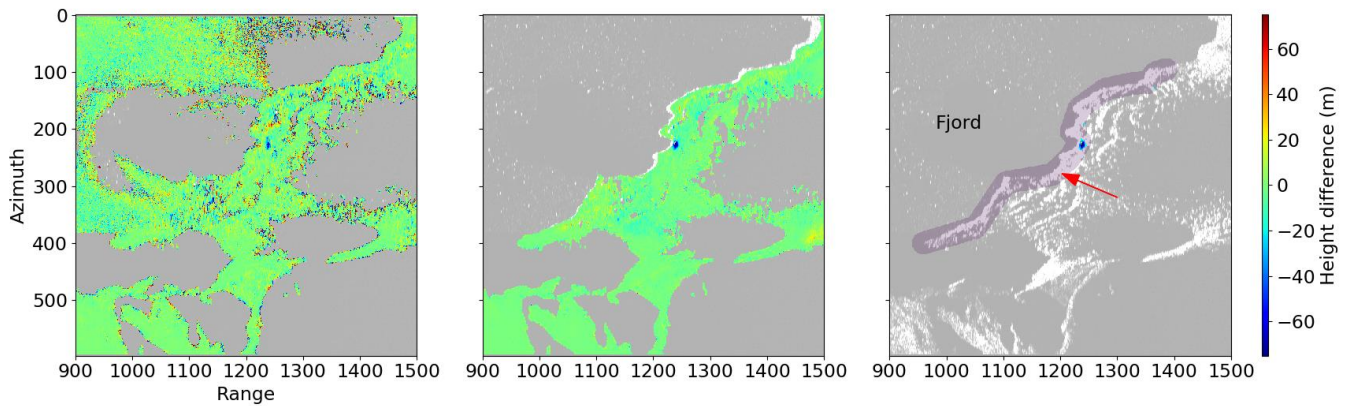


Figure 4: Example of a calving event extraction on 20 August 16:40 UTC in radar geometry. The left image shows the elevation difference between two unstacked DEMs, while in the middle the difference is calculated between two stacked DEMs. The right image shows the final extracted calving event (colours). The red arrow indicates the general flow direction of the glacier, while the purple shaded area shows the front mask.

4.2.1 Flow velocities

Ice flow velocities from TRI ~~measurements~~ data in vicinity of the calving front are presented in Figure 5.3a. Figure 5b shows the complete velocity field including the areas of ~~Due to~~ radar ~~line-of-sight~~ shadow, which has been derived additionally. Figure 3b has been created from a high resolution velocity field from repeated UAV surveys from August 2016 (Rohner et al. 2019).

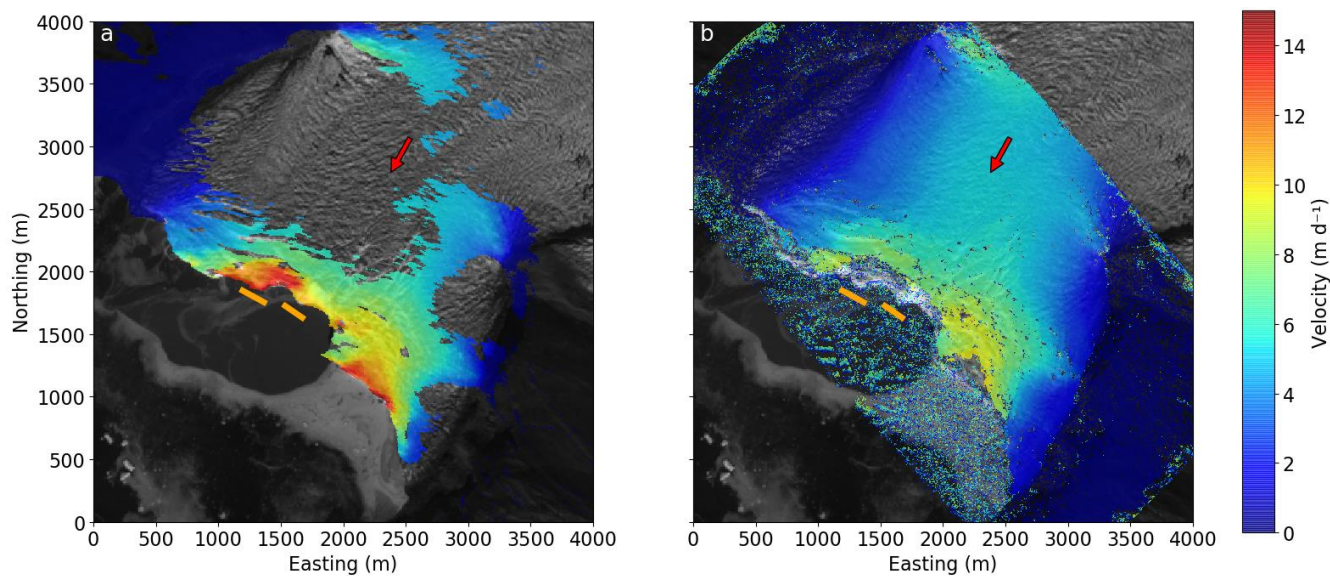
5 Speeds are increasing towards the calving front with highest values ~~of~~ reaching 16 m day^{-1} . Along the front the velocities are non-uniform, with two areas of high velocities separated by a frontal area where a bedrock ridge was visible during the field campaign (orange bar in Fig. 5.3; inset of Fig. 6.4). Further upstream the glacier velocity field is more uniform with generally higher velocities in the centre.

4.3.2 Magnitude and source area of calving events

10 During the field campaign 2016 a total of ~~906~~~~1681~~ calving events were identified within 6.12 days with a mean event volume of ~~17686~~~~1700~~ m^3 . Due to the distinctly different characteristics in cliff geometry and water depth we analysed the two front sectors ~~along the front~~ separately. Within the shallow sector ~~725~~~~1403~~ events were found, ~~while~~ ~~whereas~~ within the deep sector only ~~193~~~~289~~ events were ~~identified~~ detected, which. This results in a mean calving activity of ~~4.9~~~~9.5~~ events per hour in the shallow sector and ~~1.3~~~~2.0~~ events per hour, respectively in the deep sector. Note that ~~because~~ ~~12~~ events were detected on the border of the two sectors and were thus counted for both sectors but only once for the total number of events.

15 An overview of the ~~number~~ frequencies, volumes and event sizes is given in Table 1. The extracted ~~individual~~ calving event sizes are spread over ~~four~~~~three~~ orders of magnitude ~~from~~ $0.16 \cdot 10^3 \text{ m}^3$ up to $2.5 \cdot 10^5 \text{ m}^3$; and ~~T~~ the total volume of all calving events detected in the deep sector is ~~5.8~~~~6.6~~ times smaller than in the shallow sector. Only small variations in the position of the calving front were observed with the TRI (Fig. S1) ~~over the observation period~~, which implies that the ice loss by calving is compensated by the ice flow (Fig. 5.3).

20 Calving heights ~~differences~~ in each radar pixel (ca. 30 m^2 area) were ~~summed~~ added up over the measurement period and are referenced to as cumulative calving height. Figure 6.4 shows that within the shallow sector, the cumulative calving height locally exceeds ~~35~~~~60~~ m, while it is considerably ~~lower~~ reduced in the deep sector (D). Within the shallow sector variations in cumulative calving height are ~~also~~ observable ~~such that it can be~~ and thus this sector can be divided into four sub-sectors named SL, SM, SR and M (Figs. 6.4 and 7.5). The highest cumulative calving heights are detected ~~in~~ at sector SL, while sector M shows the lowest cumulative heights within the shallow sector. Sector SM has slightly lower values for the cumulative calving height than the sectors SR and SL. For sector D the south-eastern part next to the mainland was not in sight of the radar as it is situated behind a moraine.



5 **Figure 553:** The velocity field at the glacier front. (a) **Velocity field** measured with the TRI (line of sight) on **the** 19 August 2016 and (b) with a UAV (between 21 and 25 August 2016; Rohner et al., 2019). The red arrow indicates the general flow direction. The orange lines indicates an area where bedrock was observed at the foot of the front. The origin of the coordinate system corresponds to 528350 E / 7741550 N (UTM 22N). Background: Sentinel-2A scene from 3 August 2016 (from ESA Copernicus Science Hub: <https://scihub.copernicus.eu>).

10

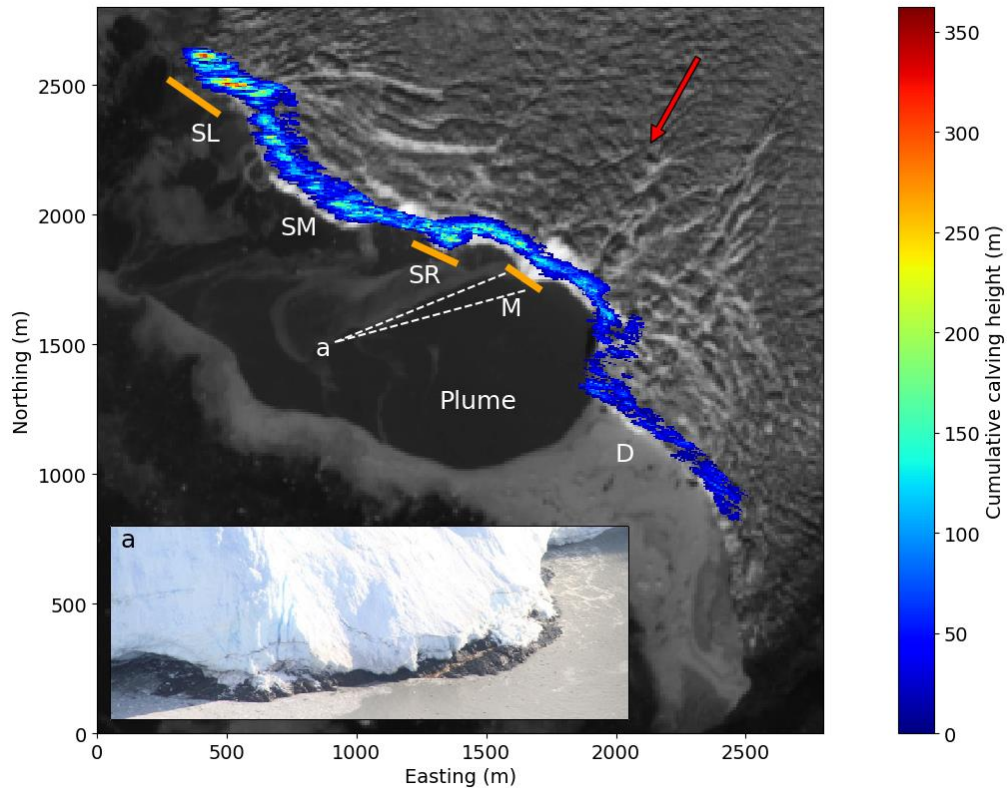
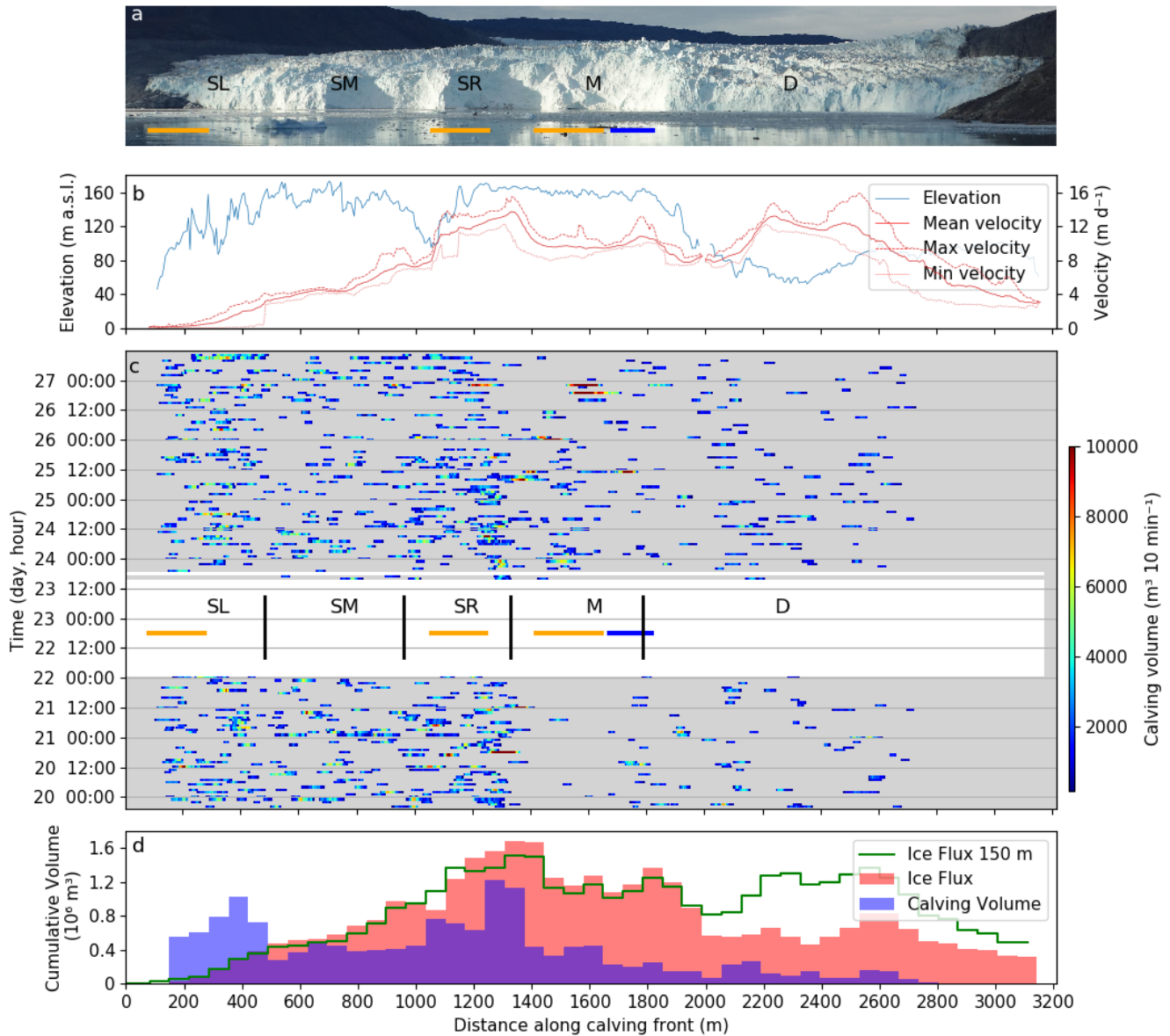


Figure 664: Spatial distribution of cumulative calving height ~~during in meters over~~ the 6 day measurement period. The capital letters correspond to the ~~different~~ sectors of the calving front (see also Fig. 5a). The deep sector (D) shows lower values than the shallow sector. Variations within the shallow sector were used to define the sectors SL, SM, SR and M. ~~The orange lines indicate areas where bedrock was observed at the basefoot of the front an example is shown, which is also shown in the inset (position and view angle of inset photograph is indicate by letter 'a' and dashed white lines respectively).~~ The freshwater plume due to subglacial discharge is well visible. Background: Sentinel-2A scene from 3 August 2016 (from ESA Copernicus Science Hub: <https://scihub.copernicus.eu>).

10 Table 1: Detected calving events within each sector during the observation period of 6.12 days.

	Whole front	Shallow sector (SL, SM, SR, M)	Deep sector (D)
Total event number	9061681	7251403	193289
Total event volume (m ³)	1602340019702000	1365580017129000	23676002573000
Event sizes			
Mean (m ³)	1770011700	1880012200	123008900
Median (m ³)	116009800	1290010200	85007400
Minimum (m ³)	660160	660250	2115160

Maximum (m ³)	275700 248900	275700 248900	108900 101800
---------------------------	--------------------------	--------------------------	--------------------------



- 5 Figure 775: The calving front of Eqip Sermia with all calving volume measurements. (a) The calving front with indication of sectors with specific calving behaviour. The differences in geometry of between the sectors SL, SM, SR (steep) and the sector D (flat) are well visible. (b) Elevation and velocity of the cliff top along the glacier front show strong variations. (c) Observed calving volumes in m³ along the front over time (20 to 27 Aug. 2019). In the data gap (white area) the corresponding front sectors are marked. The orange lines indicate bedrock outcrops and the blue line represents the location of the meltwater plume. (d) Cumulative calving volume and ice flux (per bin width of 55 m) in m³ along the front. The ice flux is calculated with the corresponding front height above sea level and velocity and with an assumed ice thickness of 150 m (termed as 'Ice Flux 150 m'). The right axis shows the percentage of calving volume with respect to the average of sectors SL, SM, SR. 50 % and 100 % are indicated as red dashed lines.
- 10

Figure 7.5 shows the detailed record of calving activity ~~in~~ along the different sectors of the calving front. Figure 7.5b presents how frontal height and velocity vary. The front height is fluctuating strongly along the front due to the highly crevassed surface. The frontal cliff in the deeper sector D is mostly vertical and between 50 and 980 m high, while in the shallow sector the front is inclined at a slope of 50 degrees and reaching up to 170 m. In general, as ~~shown already observed~~ in Figure 5.3, the velocities at the front increase from the margins towards the centre, with the exception of the area around the bedrock outcrop in sector M where velocities are slightly decreased.

Figure 7.5c summarizes the observed calving activity with event volumes and ~~tim~~ing~~es~~. The spatial pattern reflects the pattern shown on the map of cumulative calving height (Fig. 6.4). In sector D fewer and smaller events were observed than in the sectors SL, SM and SR. The four subsectors of the shallow front show well distinguishable calving event volume patterns throughout the observation period. In the central, very shallow sector M ~~less calving events were observed, but several of them are significantly larger than those observed in the other sectors. only episodic calving with large volumes was observed.~~ Interestingly, the cumulative calving height in this area is almost ~~three times a factor 3~~ smaller ~~than~~ as compared to the other shallow sectors ~~SL and SR~~ and similar to the values observed in the deep sector D. Sector SL with the highest cumulative calving height also has ~~a~~ ~~the~~ ~~large~~ ~~number~~ ~~of~~ ~~events~~ ~~most~~ ~~individual~~ ~~events~~, but they are substantially smaller than for sector M.

Figure 7.5c shows continuous calving activity without any clear temporal pattern throughout the different sectors. The only ~~visually~~ observable cluster of calving events was detected on 26 August in the afternoon, when a phase with many big events in the sectors M and SR occurred. ~~An important strong~~ spatial ~~variability variation in~~ observable calving ~~activity volumes and fluxes~~ along the front is ~~clearly~~ visible in Figure 7.5d. The shallow sectors SL and SR contribute the highest volumes, whereas only little calving was observed in the deep sector D.

Given the observations of Figure 7.5d the important question arises of how much ice mass loss at the calving front remained undetected by the TRI. Assuming ~~constant similar~~ mass flux~~es~~ over the front ~~and~~, a constant front position, ~~and assuming that the TRI detects all calving volumes in the shallow sectors, less than~~ ~~only about 10~~25% of the mass loss is detected in sector D.

4.4.3 Calving ~~event size distribution~~ ~~statistics~~

The sizes of the calving events from the different sectors were analysed statistically with the methods described in section 3.1. ~~The calving event size distribution was compared with non-linear fitting models to investigate if a self-organised critical system can be observed.~~ The event size statistics ~~for the calving events~~ were studied separately for the shallow sectors (SL, SM, SR, M) and the deep sector D and are shown in Figure 8.6. The distributions of the event sizes differ substantially between the shallow and the deep sector in the number of events (Fig. 8.6a and b), whereas the shapes of the event size distributions are similar. This results in a much lower cumulative volume of sector D, illustrated by the blue lines in Figures 8.6a and b. The result of the maximum-likelihood method is shown in ~~the~~ Figures 8.6c and d. ~~The maximum-likelihood method uses the two values R and p to describe the best fit. The probability value p should be > 0.1 and tells if one can trust the sign of the log-~~

likelihood ratio R . If R is positive the first model fits better, while if it is negative the second model is more likely. ~~The distribution of the deep sector shows a long tail and resembles a power law with an exponent $\alpha = 3.9$ (Fig. 6d). Both the power law and the log-normal model seem to explain well the event size distribution for both, the shallow and the deep sector. Comparing the different models to test, which model can describe the observed event size distribution better, results in a better~~

5 ~~fit of the log-normal model for the shallow sector ($R = -1.2$, $p = 0.1$) The distribution of the shallow sector follows more closely a log-normal distribution (Fig. 86c). The event size distribution of the deep sector is better represented by a log-normal model than by an exponential model ($R = 4.7$, $p = 0.4$), but comparing the power-law and the log-normal model shows no significant better representation ($R = -8.0$, $p = 0.02$). -but the log-likelihood ratio R and the probability value p between power law and log-normal is quite small. Therefore, the log-normal model cannot explain the event size distribution of the shallow sector~~

10 ~~perfectly.~~

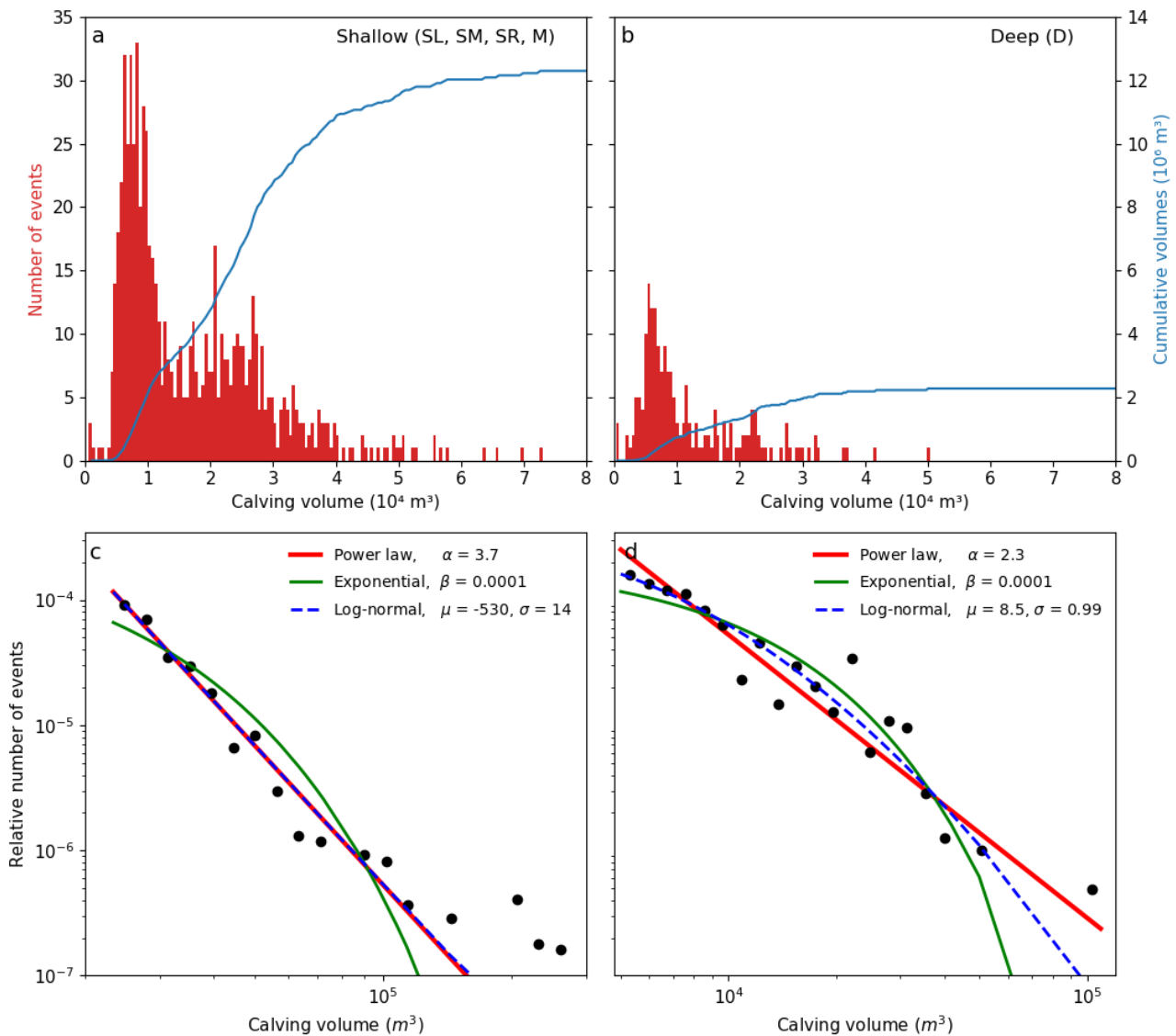


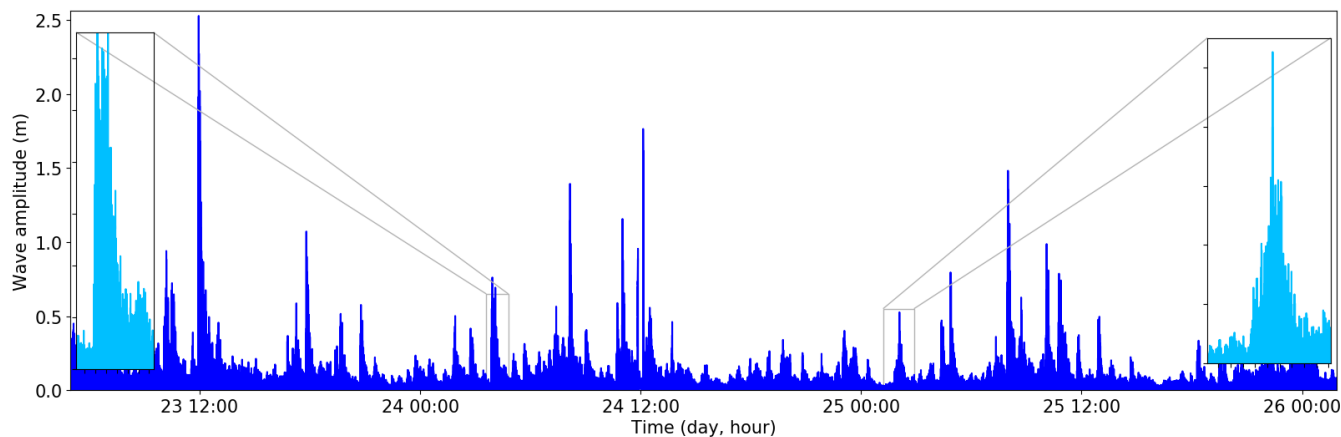
Figure 886: Event size statistics of the observed calving events. (a) The size distribution of the calving events for the shallow sector (b) and the deep sector. (c) Distributions of calving event sizes for the shallow (d) and the deep sectors. Blue, red and green lines represent the best fit power law, exponential and log-normal distribution.

5

4.5.4 Pressure sensor records

Figure 97 shows the time series of short-term variations in the fjord water levels caused by calving events, and recorded by the pressure sensor. The calving waves have an amplitude of up to 3.3 m and their duration ranged between several minutes up to about 50 min (Fig. S102). These wave events are caused by in response to single

larger calving events and are recorded with a time delay of 3-4 min. ~~Often~~ The calving-induced wave events are often difficult to attribute to single calving events due to reflection from fjord sides and superposition with subsequent events. ~~overlay each other and render it difficult to distinguish between subsequent events.~~ Two types of wave oscillations can be observed: The first and most common type has a sharp onset immediate peak in wave amplitudes water height, which are slowly damped and ~~a slow decrease with time~~ (left inset of Fig. 97). The second type is more symmetric with a gradual increase and decrease of wave amplitude (right inset of Fig. 97).



10 **Figure 997: Calving waves detected with a pressure sensor. The light blue inset panels show details of the two wave types due to calving events. The left one has a sharp onset immediate peak, while the right one shows gradual increase and decrease of wave amplitude.**

5 Discussion

15 Using a terrestrial radar interferometer we established ~~were able to produce~~ a detailed and continuous 6-~~12~~ day record of calving event volumes along the whole calving front. The detected calving event volumes were highly variable and ranged over ~~four~~three orders of magnitude, consistent with other studies of grounded tidewater glaciers (Chapuis and Tetzlaff, 2014; Pętllicki and Kinnard, 2016; Minowa et al., 2018). The observed calving events show no obvious temporal or spatial pattern, except for a series of bigger events on 26 August. ~~several clusters of events in time (e.g. on 26 August) but no clear temporal pattern of tidal or diurnal recurrence could be detected.~~

20 5.1 Relation to ice flux ~~and other processes~~

The detected total calving volume is smaller than ~~agrees with~~ the ice fluxes estimated from the flow speeds and the frontal ~~height~~ice thicknesses except for sector SL, where the calving volume is too high (Figs. 7d3 ~~and 5~~). For the sectors SM and SR the detected cumulative calving volume is about 65% of the estimated ice flux, while for sector M the calving volume is about

25% of the estimated ice flux. For sector D the cumulative calving volume is only about 15 % of the estimated aerial ice flux, while for an assumed total front thickness of 150 m the ice flux is 90% larger than the calving volume. Assuming a total ice thickness of 150 m for both sectors to calculate the total ice flux seems reasonable as this corresponds to the approximate height of the shallow section and no signs of changes in the ice flux and ice thickness can be seen upstream of the glacier.

5 Using a mean ice flow velocity of 10 m/day, a front height of 150 m and a front width of 2900 m (the part of the front observable with the TRI) a total ice flux of $4.35 \cdot 10^6 \text{ m}^3$ per day is estimated, which results over the 6.12 day period of observations in a total volume of $26.6 \cdot 10^6 \text{ m}^3$ of ice delivered to the calving front. This value should match up to the observed total calving volume of $19.7 \cdot 10^6 \text{ m}^3$, given the front position is relatively stable (Fig. S1). Total ice flux for the shallow (width 1800 m) and deep sectors (width 1100 m) amounts to $17 \cdot 10^6 \text{ m}^3$ and $10 \cdot 10^6 \text{ m}^3$, respectively. The total calving volume measured with the TRI is for the shallow sector with $17.1 \cdot 10^6 \text{ m}^3$ (Table 1) almost identical, while for the deep sector the observed calving value is with $2.6 \cdot 10^6 \text{ m}^3$ about 4 times lower than the estimated volume from ice flux. Thus ~~This suggests that,~~ within the deep sector a large fraction of the ice removed at the terminus is missing from the TRI-calving detection. ~~The filtering of calving events smaller than 160 m^3 and the stacking over 10 min intervals might contribute to this missing volume, but this underestimation of calving volume is also inherent in the shallow sector and therefore is estimated to be rather small.~~ This

10 missing calving volume ~~of $17.7 \cdot 10^6 \text{ m}^3$ within the deep sector of $7.4 \cdot 10^6 \text{ m}^3$~~ can be explained by ~~three~~two main processes. First, ~~the~~is missing volume may be removed by oceanic melt below the water line. The relatively warm saline water provides energy for ice melt where there is contact. Oceanic melt has been shown to be an important process in the mass balance of Greenland's glaciers with estimates of summer melt rates at Eqip Sermia of 0.7 m day^{-1} for 2008 (Rignot et al., 2010). Assuming an ice thickness of 100 m below the water line for ~~the deep~~ sector D this would result in a total oceanic melt volume

20 of $0.47 \cdot 10^6 \text{ m}^3$ during the observation period. However, Beard et al. (2015) showed that this estimate is likely too small as they found a ratio of surface melt ~~water~~ derived ~~water~~ to submarine melt of 26% within the fjord, which would result in higher submarine melt rates of 4 m day^{-1} when considering the melt water discharge in summer of Rignot et al. (2010). This higher melt rate would ~~over the observation period~~ result in a total mass loss through oceanic melt of $2.7 \cdot 10^6 \text{ m}^3$, which is however still substantially smaller than the ~~above~~ estimate of the ice flux for the shallow sector (Fig. 7d). ~~There,~~At the shallow sector

25 oceanic melt is ~~likely~~ less pronounced as the contact area exposed to ocean water is ~~with a water depth between 0 and 20 m~~ much smaller.

The second process explaining the missing volume is subaqueous calving, which cannot be detected with the TRI. ~~In-situ~~Visual observations by the authors and inspection of high-rate time-lapse camera imagery (Fig. 10) indicate that subaqueous calving is a frequent process but only occurs ~~at the deep~~in sector D ~~of the front~~.

30 ~~The third process is frequent calving of small volumes. Filtering of the TRI-data for event sizes smaller than 660 m^3 leads to a reduction of uncertainty but discards the potentially frequent small events below the detection limit. At the deep sector small, not detectable events are likely more frequent and contribute more to the cumulative volume due to undercutting of the calving front caused by oceanic melt. If the missing volume is indeed dominated by undetected small calving events, our data would suggest that the calving style in the deep sector is dominated by very small but frequent calving events.~~

The calving at southern side of sector M may also be affected by undercutting through enhanced submarine melt caused by the subglacial meltwater plume (blue bar in Figs. 6 and 7; Fried et al., 2015; Fried et al., 2019) and produce small and undetectable but frequent calving events. Indeed, the TRI record only shows a few small events and two larger events on 20 and 25 August resulting in low total cumulative calving volumes (Fig. 7d).

- 5 In summary, for the deep sector the three processes of oceanic melt, subaqueous calving and calving events with small volumes provide together up to 90 % of the mass removal, while for the shallow sector calving of small volumes dominates and would explain the missing volume of about 35 – 40 %.

~~If these simple estimate for ice flux in the deep and shallow sector holds and the filtered out volumes from the small events (noise) remain small in comparison, the ocean melt together with the subaqueous calving would provide 75 % of the frontal mass removal from the deep sector.~~

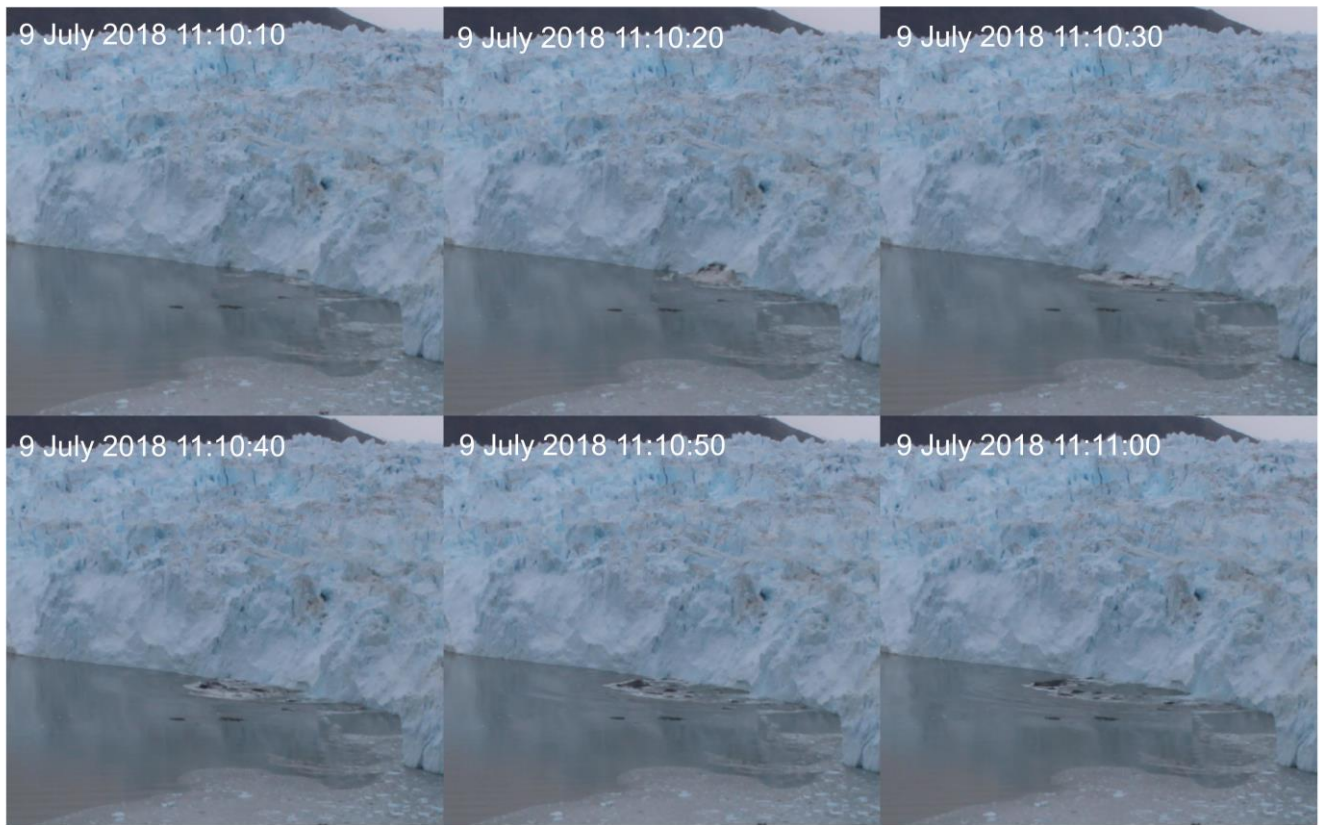


Figure 10: An example of a subaquatic calving event recorded with a time lapse camera in 2018. Pictures were taken every 10s.

5.2 Influence from cliff height and shape

- 15 The shallow sector of the front with an inclined and higher ice cliff not only shows more but also larger calving events than the deep sector. This can be explained by the different geometries, which have an impact on the calving type as the stress

regime is different. Mercenier et al. (2018) showed that an inclined ice cliff results in lower stresses, which can result in larger stable heights of the ice cliff and as a consequence at the shallow sector the calving events can release larger ice volumes. At the vertical front of the deep sector therefore smaller calving events are expected, which consistent with the observations may not be detectable with the TRI. Further, our calving event record suggests that the geometry of the front (cliff height, and slope and water depth) has an important control on the calving type. Calving events in the deep sector mostly occur as whole blocks or towers that fall into the water (visual observation by the authors). In contrast, for the sectors SL, SM, SR and M the calving events can be described mostly as avalanche like blocks or seracs that are shearing off.

The higher volumes and frequency detected for the sector SL (Fig. 75) can be explained by a rock ridge below the front of this sector. ~~Due to this rock ridge~~ There, the waterfjord is very shallow and calving can be detected over almost the full frontal thickness. The strongly episodic but very large calving events in sector M (Fig. 75) might be related to a rock ridge, over which the front is pushed (Fig. 64). Mercenier et al. (2018) found that for a smaller~~decreasing~~ water level in front of the glacier crevasses ~~stress maxima~~ tend to open ~~reach~~ further upstream and hence likely larger calving sizes occur. ~~the glacier, which causes larger calving event sizes.~~

~~The foot of the front on the southern side of sector M may be affected by the subglacial meltwater plume surfacing in this area (blue bar in Figs. 4 and 5). Here only a few small events and two larger events on 20 and 25 August can be detected, which also results in low total cumulative calving volumes (Fig. 5d). The formation of a subglacial meltwater channel can lead to undercutting of the calving front due to enhanced submarine melt (Fried et al., 2015), which then may lead to very small events, which are not detectable with the TRI.~~

5.3 Calving event size distribution ~~Calving statistics~~

The size distribution of calving events ~~is best approximated by a power law for the deep front, while~~ for the shallow and the deep front are well represented by both a log-normal and a power law model. A comparison between the two models using the maximum-likelihood method indicates that the shallow sector is better represented by a log-normal model, while for the deep sector none of the two models fits significantly better than the other. ~~seems to better fit the data~~ (Fig. 86c and d). The power law exponent of the deep sector is with $\alpha = 2.33.9$ in the range of ~~rather large compared to~~ other studies, which found an exponent between 1.2 and 2.1 (Chapuis and Tetzlaff, 2014; Åström et al., 2014; Pełlicki and Kinnard, 2016). ~~This could be explained by the missing subaqueous calving events. Observed subaqueous calving events were rather large in volume, which could lead to a lower power law exponent.~~

~~As for the deep sector the event size distribution can be represented by a power law model, it is possible that this sector of the front has the characteristics of a self-organized critical system. Those systems are characterised by a slow accumulation of an instability with small, rare events followed by a fast relief of the stresses through events of all magnitudes (Åström et al., 2014). If the deep sector behaves as a self-organized critical system calving event sizes of all magnitudes have to be expected at any time.~~

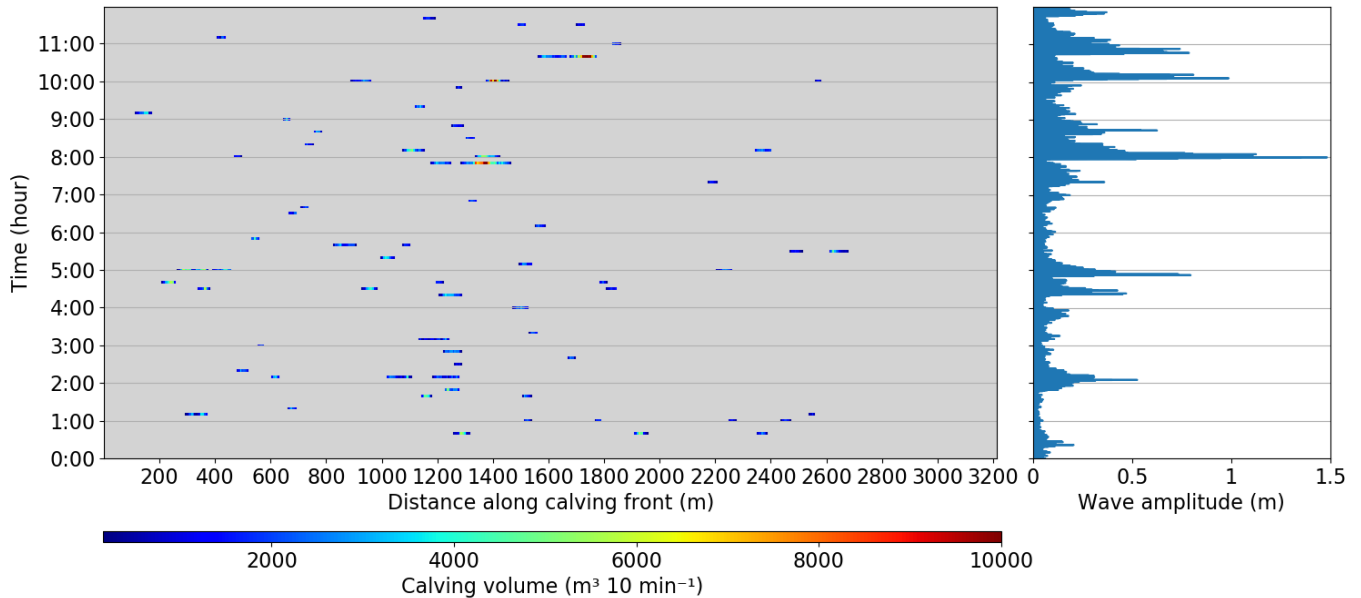
As for the shallow sector the event size distribution can be better represented by a log-normal model, it is unlikely that this sector has the characteristics of a self-organized critical system. However, for the deep sector this cannot be excluded as neither the log-normal nor the power law model is significantly better. Other studies found a clearer power-law distribution and concluded that the calving process shows characteristics of a self-organised critical system (Chapuis and Tetzlaff, 2014; Åström et al., 2014; Petlicki and Kinnard, 2016). ~~For the shallow front the event sizes tend to follow a log-normal distribution, which~~ A potential difference between the shallow and the deep sector in the event size distribution leads to the suggestion that the ~~dominant acting~~-mechanisms of break-off ~~at this sector of the front~~ are different, ~~than for the deep sector~~. This suggestion seems reasonable as for the shallow front the contact area exposed to sea water is smaller and thus submarine calving less important. A study of Kirkham et al. (2017) supports those findings as they suggest ~~s~~ by looking at size distribution of icebergs that a reduction of the number of mechanisms in their disintegration and thus a ~~lower~~~~simplifying~~ complexity leads to the transition from power law to log-normal distributions. To verify this suggestion and for a clear assignment of the deep sector to one of the proposed models more events would be needed. Also the event size distribution might change if a longer observation period is used as the calving activity is not constant over time.

5.4 Comparison with pressure sensor data

15 Figure ~~11~~~~8~~ shows a comparison of pressure sensor data and detected calving events during a 12 hour period. In addition, in Figure 12 peaks detected in the wave amplitudes are shown in comparison with the TRI derived calving events. Bigger events are clearly visible in both data sets. In the pressure sensor data, ~~t~~hose events ~~look~~ mostly ~~like~~ are of the first asymmetric type described in section 4.5.4 and displayed in Figure ~~9~~~~7~~. The second symmetric type can be found in the pressure sensor data, but in general, ~~mostly~~ they cannot be clearly assigned to a single event in the TRI dataset. These ~~symmetric events~~wave peaks, 20 like the one at 2:00 on 25 August (Fig. ~~11~~~~8~~), likely are due to larger subaqueous calving events in the deep sector as detected by the time-lapse camera (Fig. 10) (Sect. 5.1) with big up-floating icebergs that cannot be detected by the TRI. These subaquatic calving events could explain parts of the missing calving volume. This reasoning is supported by other studies who found that ~~sub~~aerial events have a gradually decreasing amplitude after the maximum wave amplitude, while subaqueous calving events showed no clear onset and a sudden drop of the amplitude after the maximum wave amplitude (Minowa et al., 25 2018). Also an experimental study showed that for aerial events the largest wave is earlier than for buoyancy driven events (Heller et al., 2019). For verification of this distinction between subaquatic and ~~sub~~aerial calving events additional observations, such as time-lapse cameras with a high temporal resolution, would be required.

In summary, the pressure sensor data together with the calving volume record (Fig. ~~11~~~~8~~) indicate that large events can be well detected from pressure sensor data. Thus, ~~potentially~~ pressure sensor observation could be exploited as a simple method to 30 derive calving event numbers, volumes and potentially even calving style (~~sub~~aerial or subaqueous). However, the analysis of

[pressure sensor data remains challenging as subglacial hydrological events, overturning of icebergs and superposition of reflected signals also produce waves and obstruct the recorded signal.](#)



5 **Figure 1118:** Comparison between pressure sensor derived wave amplitudes (right) and detected calving events (left) for a 12 hour period on 25 August. Big calving events are clearly visible in both data sets.

5.5 Relation to external forcings

Calving activity has been hypothesized to be triggered by external forcings such as [changes in stress state due to tides](#) (Bartholomäus et al., 2015) and melt water accumulation in crevasses (Benn et al., 2007). ~~and changes in stress state due to tides (Bartholomäus et al., 2015).~~ Therefore, calving activity ~~should~~ [might](#) be linked to high air temperatures and incoming radiation leading to surface melt.

Figure 129 compares air temperature, incoming shortwave radiation and tides with volume and number of calving events for the second part of the observation period (the first part is shown in Fig. S113). This comparison does not show any ~~obvious~~ [clear](#) relationship, ~~but As as~~ the observation time of 6 days is rather short, ~~we cannot exclude the influence of environmental forcings even if no significant correlations between detected events and environmental forcings are obtained, it does not exclude an influence~~ on the calving activity. Consistent with our observations, Pętllicki and Kinnard (2016) and Chapuis and Tetzlaff (2014) also found that the calving activity during their observation period of a few days was not dependent on environmental forcings, while others found an influence of ocean temperature on calving activity over seasonal timescales (Luckman et al., 2015; Schild et al., 2018).

20

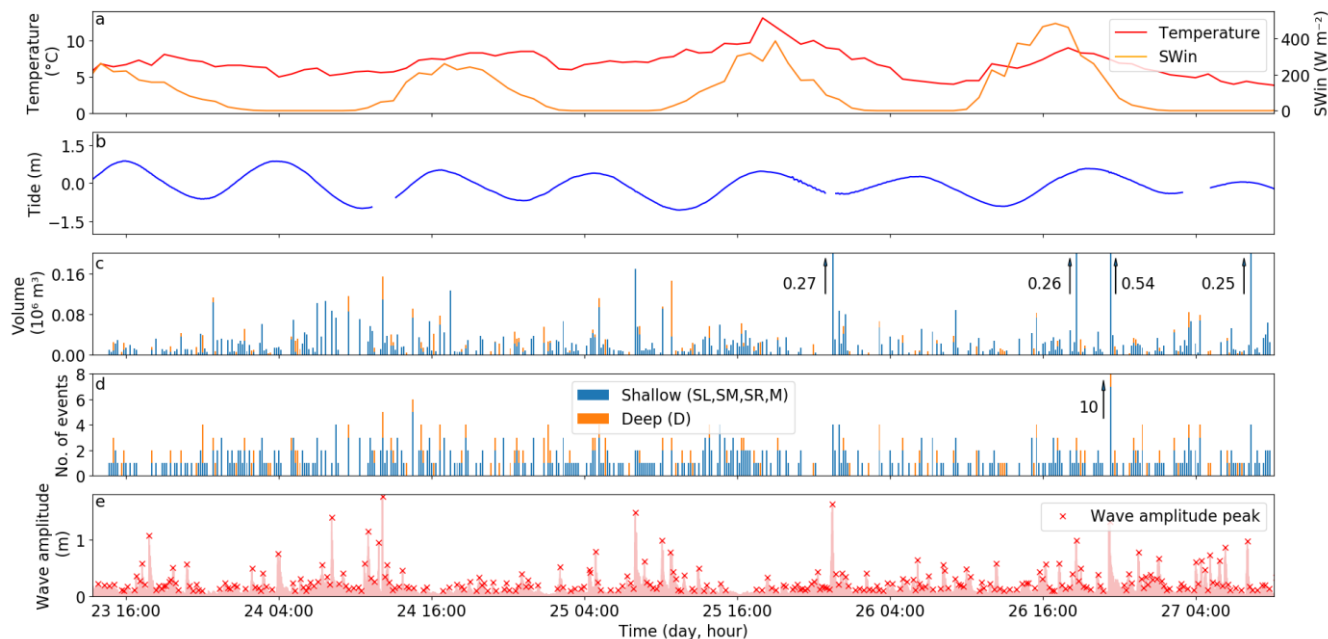


Figure 12129: Comparison between forcing and detected calving during a 3 day period. (a) Air temperature and incoming shortwave radiation from the AWS1 for the second part of the observation period. (b) Incoming shortwave radiation. (c) Tidal range in meters. (d) Volume of calving events in m^3 for the shallow and deep sectors. (e) Number of calving events. The calving events in the deep sector are plotted above those in the shallow sector. (e) Pressure sensor derived wave amplitudes and detected peaks.

6 Conclusion

We developed a novel method to establish a detailed, spatially resolved calving event catalogue and statistics and to quantify calving volumes and source areas. During 6 days 1681 calving events were identified for the whole calving front of which 85% in the shallow sector. Calving events of the shallow sector have a larger mean volume of 12200 m^3 as compared to 8900 m^3 for the deep sector. Assuming similar ice flux in both sectors the missing calving volume of the deep sector has to be explained by other processes than aerial calving. Our analysis shows that in the deep sector the mass loss due to subaqueous calving and oceanic melt likely contributes 75 % to the total mass loss. The event size distributions of the two sectors follow a power law and a log normal model, respectively. The variations of the calving event sizes and number of events for the different sectors can be explained by the bed topography and the calving front geometry. The shallow sector is characterised by an inclined front and shows a different calving type than the deep sector and calving events can release larger ice volumes. A rock ridge in the center of the calving front influences the calving activity and leads to fewer but larger events. Comparing the detected calving events with pressure sensor data shows that the big events are clearly discernible in both data sets. Some events in the pressure sensor data, which are not visible in the TRI data, show a different shape in the wave

~~oscillation and likely correspond to subaqueous calving events. For the short time span of the observations no relationship between the observed calving activity and environmental forcings (tides, temperature, incoming shortwave radiation) could be established.~~

~~This study shows the potential of detailed high-rate observations to elucidate the processes and forcings leading to iceberg calving from tidewater glaciers. The resulting statistics of calving event sizes in relation to geometry, bathymetry and external forcings are important benchmarks for calving models. Testing and calibrating such models with field data is mandatory for the understanding of the delicate dynamics of outlet glaciers which control the dynamics of large parts of the Greenland ice sheet.~~

We developed a novel calving detection method applicable to high-rate TRI scans of glacier calving fronts. By differencing high-resolution DEMs generated from the TRI data, a detailed calving event catalogue was established, providing timing, source area and calving volume of aerial calving events.

The calving front of the observed glacier is characterized by sectors of different water depth and front height. The shallow sector features an inclined front, and frequent calving events release larger ice volumes, whereas the deep sector produces less and smaller icebergs. A rock ridge in the centre of the calving front influences the calving activity there and leads to fewer but larger events.

During the 6 day observation period a total of 906 calving events were detected, of which 80% occurred in the shallow sector where mean calving volumes were 35% larger than in the deep sector. Since ice flux in both sectors is of similar magnitude, processes other than aerial calving seem to remove an important fraction of ice in the deep sector. Our analysis shows that the mass loss due to subaqueous calving, oceanic melt, and small aerial calving events contribute 90% to the total mass loss. Further, the event size distribution differs between the sectors, and fits a log-normal model in the shallow sector, whereas for the deep sector both a log-normal and a power law model fit well but none significantly better. These differences in calving behaviour are clearly linked to basal topography and calving front geometry.

Comparison of the calving events with wave data registered with a pressure sensor shows that big events are clearly discernible in both data sets. Several events detected in the wave record, that do not occur in the TRI data, show a different wave characteristic, and likely correspond to subaqueous calving events. For the time span of the observations no obvious relationship between the observed calving activity and environmental forcings, such as tides, temperature and incoming shortwave radiation, could be established.

This study shows the potential of detailed high-rate observations to elucidate the processes and forcings leading to iceberg calving from tidewater glaciers. The resulting statistics of calving event sizes in relation to geometry, bathymetry and external forcings are important benchmarks for calving models. Testing and calibrating such models with field data is mandatory for the understanding of the delicate dynamics of outlet glaciers which control the evolution of large parts of the Greenland ice sheet.

Code and data availability. Data and codes are available from the authors upon request.

Competing interests. The authors declare that they have no conflict of interest.

Acknowledgments. [We thank Diego Wasser and Rémy Mercenier for help during the field campaign at Eqip Sermia and Gamma Remote Sensing AG for the support during the data analysis. We acknowledge the reviews by Surui Xie and Pierre-Marie Lefeuvre and the additional comments by the scientific editor, which were of great help when revising the paper and have significantly improved its quality. This work was funded by University of Zurich and ETH Zurich, Switzerland. The field work was supported through grants 200021-156098 and 200021-153179/1 of the Swiss National Science Foundation.](#)~~We thank Diego Wasser and Rémy Mercenier for help during the field campaign at Eqip Sermia. This work was funded by University of Zurich and ETH Zurich, Switzerland. The field work was supported through grants 200021-156098 and 200021-153179/1 of the Swiss National Science Foundation.~~

10 *Author contributions.* A. Walter, M. P. Lüthi and A. Vieli designed the manuscript. A. Walter performed all analysis and wrote the draft of the manuscript. All authors contributed to the final version of the manuscript.

References

- Alstott, J., Bullmore, E., and Plenz, D.: powerlaw. A Python package for analysis of heavy-tailed distributions, *PloS ONE* 9 (1): e85777, <https://doi.org/10.1371/journal.pone.0085777>, 2014.
- 15 Amundson, J. M., Clinton, J. F., Fahnestock, M., Truffer, M., Lüthi, M. P., and Motyka, R. J.: Observing calving-generated ocean waves with coastal broadband seismometers, Jakobshavn Isbræ, Greenland, *Ann. Glaciol.* 53 (60), 79–84, <https://doi.org/10.3189/2012/AoG60A200>, 2012.
- Åström, J. A., Vallot, D., Schäfer, M., Welty, E. Z., O’Neel, S., Bartholomäus, T. C., Liu, Yan, Riikilä, T. I., Zwinger, T., Timonen, J., and Moore, J. C.: Termini of calving glaciers as self-organized critical systems, *Nature Geoscience* 7 (12), 874–
20 878, <https://doi.org/10.1038/NGEO2290>, 2014.
- Bartholomäus, T. C., Larsen, Ch. F., O’Neel, S., and West, M. E.: Calving seismicity from iceberg-sea surface interactions, *J. Geophys. Res.* 117 (F4), <https://doi.org/10.1029/2012JF002513>, 2012.
- Bartholomäus, T. C., Larsen, Ch. F., West, M. E., O’Neel, S., Pettit, E. C., and Truffer, M.: Tidal and seasonal variations in calving flux observed with passive seismology, *J. Geophys. Res. Earth Surf.* 120 (11), 2318–2337,
25 <https://doi.org/10.1002/2015JF003641>, 2015.
- Beaird, N., Straneo, F., and Jenkins, W.: Spreading of Greenland meltwaters in the ocean revealed by noble gases, *Geophys. Res. Lett.* 42 (18), 7705–7713, <https://doi.org/10.1002/2015GL065003>, 2015.

- Benn, D. I., Warren, Ch. R., and Mottram, R. H.: Calving processes and the dynamics of calving glaciers, *Earth-Science Reviews* 82 (3-4), 143–179, <https://doi.org/10.1016/j.earscirev.2007.02.002>, 2007.
- Caduff, R., Schlunegger, F., Kos, A., and Wiesmann, A.: A review of terrestrial radar interferometry for measuring surface change in the geosciences, *Earth Surf. Process. Landforms* 40 (2), 208–228, <https://doi.org/10.1002/esp.3656>, 2015.
- 5 Carr, R. J., Bell, H., Killick, R., and Holt, T.: Exceptional retreat of Novaya Zemlya's marine-terminating outlet glaciers between 2000 and 2013, *The Cryosphere* 11 (5), 2149–2174, <https://doi.org/10.5194/tc-11-2149-2017>, 2017.
- Cassotto, R., Fahnestock, M., Amundson, J. M., Truffer, M., Boettcher, M. S., de la Pena, S., and Howat, I.: Non-linear glacier response to calving events, Jakobshavn Isbræ, Greenland, *J. Glaciol.* 4, 1–16, <https://doi.org/10.1017/jog.2018.90>, 2018.
- Catania, G. A., Stearns, L. A., Sutherland, D. A., Fried, M. J., Bartholomäus, T. C., Morlighem, M., Shroyer, E., and Nash, J.:
10 Geometric Controls on Tidewater Glacier Retreat in Central Western Greenland, *Journal of Geophysical Research: Earth Surface*, 123, 2024–2038, <https://doi.org/10.1029/2017JF004499>, 2018.
- Chapuis, A., Rolstad, C., and Norland, R.: Interpretation of amplitude data from a ground-based radar in combination with terrestrial photogrammetry and visual observations for calving monitoring of Kronebreen, Svalbard, *Ann. Glaciol.* 51 (55), 34–40, <https://doi.org/10.3189/172756410791392781>, 2010.
- 15 Chapuis, A., and Tetzlaff, T.: The variability of tidewater-glacier calving. Origin of event-size and interval distributions, *J. Glaciol.* 60 (222), 622–634, <https://doi.org/10.3189/2014JoG13J215>, 2014.
- Clauset, A., Shalizi, C. R., and Newman, M. E. J.: Power-Law Distributions in Empirical Data, *SIAM Rev.* 51 (4), 661–703, <https://doi.org/10.1137/070710111>, 2009.
- 20 [Duarte, M., and Watanabe, R.N.: Notes on Scientific Computing for Biomechanics and Motor Control, GitHub repository, https://github.com/BMCLab/BMC, 2018.](https://github.com/BMCLab/BMC)
- Enderlin, E. M., Howat, I. M., Jeong, S., Noh, M.-J., van Angelen, J. H., and van den Broeke, M. R.: An improved mass budget for the Greenland ice sheet, *Geophys. Res. Lett.* 41 (3), 866–872, <https://doi.org/10.1002/2013GL059010>, 2014.
- Fried, M. J., Catania, G. A., Bartholomäus, T. C., Duncan, D., Davis, M., Stearns, L. A., Nash, J., Shroyer, E., and Sutherland, D.: Distributed subglacial discharge drives significant submarine melt at a Greenland tidewater glacier, *Geophys. Res. Lett.*
25 42 (21), 9328–9336, <https://doi.org/10.1002/2015GL065806>, 2015.

[Fried, M. J., Carroll, D., Catania, G. A., Sutherland, D. A., Stearns, L. A., Shroyer, E., and Nash, J.: Distinct frontal ablation processes drive heterogeneous submarine terminus morphology, *Geophysical Research Letters*, 46, <https://doi.org/10.1029/2019GL083980>, 2019.](https://doi.org/10.1029/2019GL083980)

5 Glowacki, O., Deane, G. B., Moskalik, M., Blondel, Ph., Tegowski, J., and Blaszczyk, M.: Underwater acoustic signatures of glacier calving, *Geophys. Res. Lett.* 42 (3), 804–812, <https://doi.org/10.1002/2014GL062859>, 2015.

Goldstein, R.: Atmospheric limitations to repeat-track radar interferometry, *Geophys. Res. Lett.* 22 (18), 2517–2520, <https://doi.org/10.1029/95GL02475>, 1995.

10 [Heller, V., Chen, F., Brühl, M., Gabl, R., Chen, X., Wolters, G., and Fuchs, H.: Large-scale experiments into the tsunamigenic potential of different iceberg calving mechanisms, *Scientific Reports* 9, 861, <https://doi.org/10.1038/s41598-018-36634-3>, 2019.](https://doi.org/10.1038/s41598-018-36634-3)

Holland, D. M., Thomas, R. H., de Young, B., Ribergaard, M. H., and Lyberth, B.: Acceleration of Jakobshavn Isbræ triggered by warm subsurface ocean waters, *Nature Geosci* 1 (10), 659–664, <https://doi.org/10.1038/ngeo316>, 2008.

Howat, I. M., Box, J. E., Ahn, Y., Herrington, A., and McFadden, E. M.: Seasonal variability in the dynamics of marine-terminating outlet glaciers in Greenland, *J. Glaciol.* 56 (198), 601–613, <https://doi.org/10.3189/002214310793146232>, 2010.

15 IPCC 2013 (Hg.): Climate change 2013. The physical science basis: Working Group I contribution to the Fifth assessment report of the Intergovernmental Panel on Climate Change. Cambridge: Cambridge University Press, <https://doi.org/10.1017/CBO9781107415324>, 2014.

Joughin, I., Abdalati, W., and Fahnestock, M.: Large fluctuations in speed on Greenland's Jakobshavn Isbrae glacier, *Nature* 432 (7017), 608–610, <https://doi.org/10.1038/nature03130>, 2004.

20 Jouvét, G., Weidmann, Y., Seguinot, J., Funk, M., Abe, T., Sakakibara, D., Seddik, H., and Sugiyama, S.: Initiation of a major calving event on the Bowdoin Glacier captured by UAV photogrammetry, *The Cryosphere* 11 (2), 911–921, <https://doi.org/10.5194/tc-11-911-2017>, 2017.

King, M. D., Howat, I. M., Jeong, S., Noh, M. J., Wouters, B., Noël, B., and van den Broeke, M. R.: Seasonal to decadal variability in ice discharge from the Greenland Ice Sheet, *The Cryosphere* 12 (12), 3813–3825, <https://doi.org/10.5194/tc-12-3813-2018>, 2018.

25

- Kirkham, J. D., Rosser, N. J., Wainwright, J., Vann Jones, E. C., Dunning, St. A., Lane, V. S., Hawthorn, D. E., Strzelecki, M. C., and Szczuciński, W.: Drift-dependent changes in iceberg size-frequency distributions, *Scientific reports* 7 (1), 15991, <https://doi.org/10.1038/s41598-017-14863-2>, 2017.
- 5 [Köhler, A., Nuth, Ch., Kohler, J., Berthier, E., Weidle, Ch., and Schweitzer, J.: A 15 year record of frontal glacier ablation rates estimated from seismic data, *Geophysical Research Letters*, 43, 12.155-12.164, <https://doi.org/10.1002/2016GL070589>, 2016.](#)
- [Köhler, A., Petlicki, M., Lefevre, P.-M., Buscaino, G., Nuth, C., and Weidle, C.: Contribution of calving to frontal ablation quantified from seismic and hydroacoustic observations calibrated with lidar volume measurements, *The Cryosphere*, 13, 3117–3137, <https://doi.org/10.5194/tc-13-3117-2019>, 2019.](#)
- 10 Luckman, A., Benn, D. I., Cottier, F., Bevan, S., Nilsen, F., and Inall, M.: Calving rates at tidewater glaciers vary strongly with ocean temperature, *Nature communications* 6, 8566, <https://doi.org/10.1038/ncomms9566>, 2015.
- Lüthi, M. P., and Vieli, A.: Multi-method observation and analysis of a tsunami caused by glacier calving, *The Cryosphere* 10 (3), 995–1002, <https://doi.org/10.5194/tc-10-995-2016>, 2016.
- Lüthi, M. P., Vieli, A., Moreau, L., Joughin, I., Reisser, M., Small, D., and Stober, M.: A century of geometry and velocity evolution at Eqip Sermia, West Greenland, *J. Glaciol.* 62 (234), 640–654, <https://doi.org/10.1017/jog.2016.38>, 2016.
- 15 McFadden, E. M., Howat, I. M., Joughin, I., Smith, B. E., and Ahn, Y.: Changes in the dynamics of marine terminating outlet glaciers in west Greenland (2000-2009), *J. Geophys. Res.* 116, F02022, <https://doi.org/10.1029/2010JF001757>, 2011.
- Mercenier, R., Lüthi, M. P., and Vieli, A.: Calving relation for tidewater glaciers based on detailed stress field analysis, *The Cryosphere* 12 (2), 721–739, <https://doi.org/10.5194/tc-12-721-2018>, 2018.
- 20 Minowa, M., Podolskiy, E. A., Sugiyama, S., Sakakibara, D., and Skvarca, P.: Glacier calving observed with time-lapse imagery and tsunami waves at Glaciar Perito Moreno, Patagonia, *J. Glaciol.* 64 (245), 62–376, <https://doi.org/10.1017/jog.2018.28>, 2018.
- Moon, T., Joughin, I., Smith, B., and Howat, I.: 21st-century evolution of Greenland outlet glacier velocities, *Science* (New York, N.Y.) 336 (6081), 576–578, <https://doi.org/10.1126/science.1219985>, 2012.
- 25 [Morlighem, M., Williams, C.N., Rignot, E., An, L., Arndt, J.E., Bamber, J.L., et al., *BedMachine v3: Complete bed topography and ocean bathymetry mapping of Greenland from multibeam echo sounding combined with mass conservation, *Geophysical Research Letters*, 44, 11.051-11.061, <https://doi.org/10.1002/2017GL074954>, 2017.*](#)

- Nick, F. M., Vieli, A., Howat, I. M., and Joughin, I.: Large-scale changes in Greenland outlet glacier dynamics triggered at the terminus, *Nature Geosci* 2 (2), 110–114, <https://doi.org/10.1038/ngeo394>, 2009.
- O’Neel, S., Echelmeyer, K. A., and Motyka, R. J.: Short-term variations in calving of a tidewater glacier. LeConte Glacier, Alaska, U.S.A, *J. Glaciol.* 49 (167), 587–598, <https://doi.org/10.3189/172756503781830430>, 2003.
- 5 O’Neel, S., Larsen, Ch. F., Rupert, N., and Hansen, R.: Iceberg calving as a primary source of regional-scale glacier-generated seismicity in the St. Elias Mountains, Alaska, *J. Geophys. Res.* 115, L22501, <https://doi.org/10.1029/2009JF001598>, 2010.
- Pełlicki, M., and Kinnard, Ch.: Calving of Fuerza Aérea Glacier (Greenwich Island, Antarctica) observed with terrestrial laser scanning and continuous video monitoring, *J. Glaciol.* 62 (235), 835–846, <https://doi.org/10.1017/jog.2016.72>, 2016.
- Porter, C., Morin, P., Howat, I., Noh, M.-J., Bates, B., Peterman, K., Keesey, S., Schlenk, M., Gardiner, J., Tomko, K., Willis,
10 M., Kelleher, C., Cloutier, M., Husby, E., Foga, S., Nakamura, H., Platson, M., Wethington, M., Jr., Williamson, C., Bauer, G., Enos, J., Arnold, G., Kramer, W., Becker, P., Doshi, A., D’Souza, C., Cummens, P., Laurier, F., and Bojesen, M.: “ArcticDEM”, Harvard Dataverse, V1, <https://doi.org/10.7910/DVN/OHHUKH>, 2018.
- Pralong, A., and Funk, M.: Dynamic damage model of crevasse opening and application to glacier calving, *J. Geophys. Res.* 110, B01309, <https://doi.org/10.1029/2004JB003104>, 2005.
- 15 Rignot, E., Velicogna, I., van den Broeke, M. R., Monaghan, A., and Lenaerts, J. T. M.: Acceleration of the contribution of the Greenland and Antarctic ice sheets to sea level rise, *Geophys. Res. Lett.* 38 (5), <https://doi.org/10.1029/2011GL046583>, 2011.
- Rignot, E., Fenty, I., Xu, Y., Cai, C., and Kemp, Ch.: Undercutting of marine-terminating glaciers in West Greenland, *Geophys. Res. Lett.* 42 (14), 5909–5917, <https://doi.org/10.1002/2015GL064236>, 2015.
- 20 Rignot, E., Koppes, M., and Velicogna, I.: Rapid submarine melting of the calving faces of West Greenland glaciers, *Nature Geosci* 3 (3), 187–191, <https://doi.org/10.1038/ngeo765>, 2010.
- Rohner, Ch., Small, D., Henke, D., Lüthi, M. P., and Vieli, A.: Multisensor validation of tidewater glacier flow fields derived from SAR intensity tracking, *The Cryosphere* ~~Discuss.~~, [13, 2953-2975](https://doi.org/10.5194/tc-13-2953-2019) ~~1–27~~, <https://doi.org/10.5194/tc-13-2953-2019> ~~2018-278~~, 2019.
- 25 Rolstad, C., and Norland, R.: Ground-based interferometric radar for velocity and calving-rate measurements of the tidewater glacier at Kronebreen, Svalbard, *Ann. Glaciol.* 50 (50), 47–54, <https://doi.org/10.3189/172756409787769771>, 2009.

- Schild, K. M., Renshaw, C. E., Benn, D. I., Luckman, A., Hawley, R. L., How, P., Trusel, L., Cottier, F. R., Pramanik, A., and Hulton, N. R. J.: Glacier Calving Rates Due to Subglacial Discharge, Fjord Circulation, and Free Convection, *J. Geophys. Res. Earth Surf.* 123 (9), 2189–2204, <https://doi.org/10.1029/2017JF004520>, 2018.
- Straneo, F., Heimbach, P., Sergienko, O., Hamilton, G., Catania, G. A., Griffies, S., Hallberg, R., Jenkins, A., Joughin, I., Motyka, R., Pfeffer, T. W., Price, S. F., Rignot, E., Scambos, T., Truffer, M., and Vieli, A.: Challenges to Understanding the Dynamic Response of Greenland's Marine Terminating Glaciers to Oceanic and Atmospheric Forcing, *Bull. Amer. Meteor. Soc.* 94 (8), 1131–1144, <https://doi.org/10.1175/BAMS-D-12-00100.1>, 2013.
- Strozzi, T., Werner, Ch., Wiesmann, A., and Wegmüller, U.: Topography Mapping With a Portable Real-Aperture Radar Interferometer, *IEEE Geoscience And Remote Sensing Letters* 9 (2), 277–281, <https://doi.org/10.1109/LGRS.2011.2166751>, 2012.
- Thomas, R. H.: Force-perturbation analysis of recent thinning and acceleration of Jakobshavn Isbræ, Greenland, *J. Glaciol.* 50 (168), 57–66, <https://doi.org/10.3189/172756504781830321>, 2004.
- Vallot, D., Adinogroho, S., Strand, R., How, P., Pettersson, R., Benn, D. I., and Hulton, N. R. J.: Automatic detection of calving events from time-lapse imagery at Tunabreen, Svalbard, *Geosci. Instrum. Method. Data Syst.* 8 (1), 113–127, <https://doi.org/10.5194/gi-8-113-2019>, 2019.
- van der Walt, S., Schönberger, J. L., Nunez-Iglesias, J., Boulogne, F., Warner, J. D., Yager, N., Gouillart, E., and Yu, T.: scikit-image. Image processing in Python, *PeerJ* 2, e453, <https://doi.org/10.7717/peerj.453>, 2014.
- Vieli, A., and Nick, F. M.: Understanding and Modelling Rapid Dynamic Changes of Tidewater Outlet Glaciers. *Issues and Implications*, *Surv Geophys* 32 (4-5), 437–458, <https://doi.org/10.1007/s10712-011-9132-4>, 2011.
- Voytenko, D., Stern, A., Holland, D. M., Dixon, T. H., Christianson, K., and Walker, R. T.: Tidally driven ice speed variation at Helheim Glacier, Greenland, observed with terrestrial radar interferometry, *J. Glaciol.* 61 (226), 301–308, <https://doi.org/10.3189/2015JoG14J173>, 2015.
- Walter, F., Olivieri, M., and Clinton, J. F.: Calving event detection by observation of seiche effects on the Greenland fjords, *J. Glaciol.* 59 (213), 162–178, <https://doi.org/10.3189/2013JoG12J118>, 2013.
- Walter, F., O'Neel, S., McNamara, D., Pfeffer, W. T., Bassis, J. N., and Fricker, H. A.: Iceberg calving during transition from grounded to floating ice. Columbia Glacier, Alaska, *Geophys. Res. Lett.* 37 (15), <https://doi.org/10.1029/2010GL043201>, 2010.

Warren, Ch. R.: Terminal environment, topographic control and fluctuations of West Greenland glaciers, *Boreas* 20 (1), 1–15, <https://doi.org/10.1111/j.1502-3885.1991.tb00453.x>, 1991.

Warren, Ch. R., Glasser, N. F., Harrison, S., Winchester, V., Kerr, A. R., and Rivera, A.: Characteristics of tide-water calving at Glaciar San Rafael, Chile, *J. Glaciol.* 41 (138), 273–289, <https://doi.org/10.3189/S0022143000016178>, 1995.

- 5 Werner, Ch., Strozzi, T., Wiesmann, A., and Wegmüller, U.: A Real-Aperture Radar for Ground-Based Differential Interferometry, IGARSS Conference Paper, 210-213, <https://doi.org/10.1109/IGARSS.2008.4779320>, 2008a.

Werner, Ch., Strozzi, T., Wiesmann, A., and Wegmüller, U.: Gamma's portable radar interferometer, Symposium on Deformation Measurement and Analysis, 2008b.

- 10 Xie, S., Dixon, T. H., Voytenko, D., Deng, F., and Holland, D. M.: Grounding line migration through the calving season of Jakobshavn Isbræ, Greenland, observed with terrestrial radar interferometry, *The Cryosphere Discuss.*, 1–29, <https://doi.org/10.5194/tc-2017-231>, 2018.

[Xie, S., Dixon, T.H., Holland, D.M., Voytenko D., Vaňková,I.: Rapid iceberg calving following removal of tightly packed pro-glacial mélange, *Nature Communication* 10, 3250, <https://doi.org/10.1038/s41467-019-10908-4>, 2019.](https://doi.org/10.1038/s41467-019-10908-4)